Resource

Cell

# A Living Biobank of Breast Cancer Organoids Captures Disease Heterogeneity

## Graphical Abstract

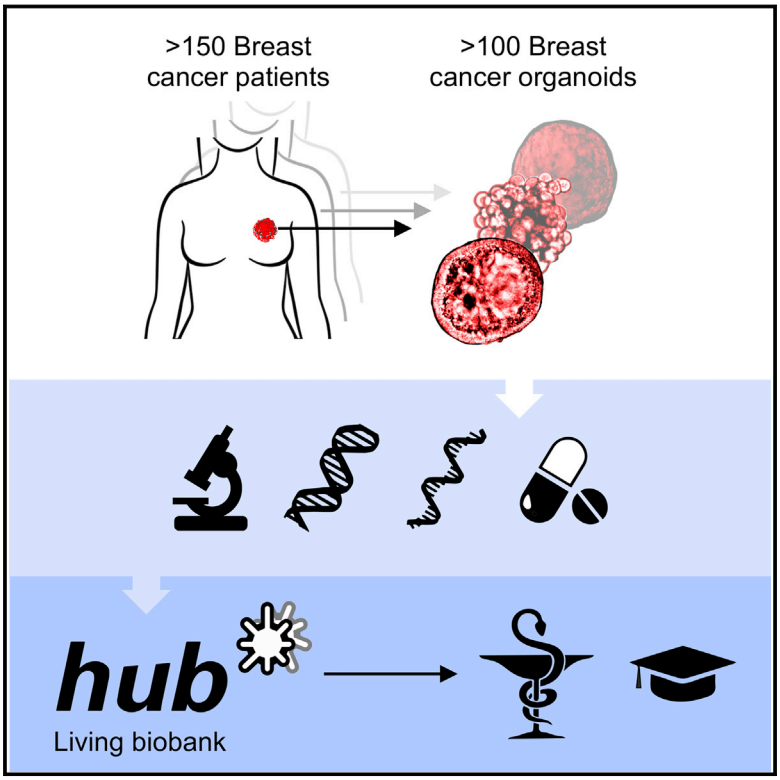


## Highlights

- Culture conditions for human mammary epithelial organoids were established
- Living biobank with >100 primary and metastatic breast cancer organoid lines
- Organoids recapitulate histological and genetic features of original tumors
- Organoids allow high-throughput drug screening and potentially aid personalized therapy

## Authors

Norman Sachs, Joep de Ligt, Oded Kopper, ..., Robert Gerhardus Jacob Vries, Edwin Cuppen, Hans Clevers

## Correspondence

h.clevers@hubrecht.eu

## In Brief

The heterogeneity of breast cancer subtypes can be captured using organoid cultures that can facilitate drug screens that corroborate with patient responses.

Sachs et al., 2018, Cell *172*, 1–14
January 11, 2018 
https://doi.org/10.1016/j.cell.2017.11.010

CellPress

Please cite this article in press as: Sachs et al., A Living Biobank of Breast Cancer Organoids Captures Disease Heterogeneity, Cell (2018), https://doi.org/10.1016/j.cell.2017.11.010

Resource

Cell

# A Living Biobank of Breast Cancer Organoids Captures Disease Heterogeneity

Norman Sachs,[1,2,11,14,15] Joep de Ligt,[3,11,14] Oded Kopper,[1,11,14] Ewa Gogola,[4] Gergana Bounova,[5,11] Fleur Weeber,[6] Anjali Vanita Balgobind,[1,2] Karin Wind,[1] Ana Gracanin,[1] Harry Begthel,[1] Jeroen Korving,[1] Ruben van Boxtel,[3,11] Alexandra Alves Duarte,[4] Daphne Lelieveld,[7] Arne van Hoeck,[3,11] Robert Frans Ernst,[3,11] Francis Blokzijl,[3,11] Isaac Johannes Nijman,[3,11] Marlous Hoogstraat,[5] Marieke van de Ven,[8] David Anthony Egan,[7] Vittoria Zinzalla,[12] Jurgen Moll,[12] Sylvia Fernandez Boj,[2,11] Emile Eugene Voest,[6] Lodewyk Wessels,[4,11,13] Paul Joannes van Diest,[9] Sven Rottenberg,[4,10] Robert Gerhardus Jacob Vries,[2,11] Edwin Cuppen,[3,11] and Hans Clevers[1,11,16,*]

[1]Hubrecht Institute, Royal Netherlands Academy of Arts and Sciences and University Medical Center Utrecht, Uppsalalaan 8, 3584 CT Utrecht, the Netherlands

[2]Foundation Hubrecht Organoid Technology (HUB), Yalelaan 62, 3584 CM Utrecht, the Netherlands

[3]Center for Molecular Medicine, Department of Genetics, University Medical Center Utrecht, Utrecht University, Universiteitsweg 100, 3584 CG Utrecht, the Netherlands

[4]Division of Molecular Pathology, Netherlands Cancer Institute, Plesmanlaan 121, 1066 CX Amsterdam, the Netherlands

[5]Division of Molecular Carcinogenesis, Netherlands Cancer Institute, Plesmanlaan 121, 1066 CX Amsterdam, the Netherlands

[6]Division of Molecular Oncology and Immunology, Netherlands Cancer Institute, Plesmanlaan 121, 1066 CX Amsterdam, the Netherlands

[7]Cell Screening Core, Department of Cell Biology, Center for Molecular Medicine, University Medical Center, Heidelberglaan 100, 3584 CX Utrecht, the Netherlands

[8]Mouse Clinic for Cancer and Aging (MCCA), Preclinical Intervention Unit, Netherlands Cancer Institute, Plesmanlaan 121, 1066 CX Amsterdam, the Netherlands

[9]Department of Pathology, University Medical Center Utrecht, Heidelberglaan 100, 3584 CX Utrecht, the Netherlands

[10]Institute of Animal Pathology, Vetsuisse Faculty, University of Bern, Länggassstrasse 122, 3012 Bern, Switzerland

[11]Cancer Genomics Netherlands, Oncode Institute, 3584 CG Utrecht, the Netherlands

[12]Pharmacology and Translational Research, Boehringer Ingelheim RCV GmbH & Co KG, Dr. Boehringer-Gasse 5-11, 1121 Vienna, Austria

[13]Faculty of EEMCS, Delft University of Technology, Delft, the Netherlands

[14]These authors contributed equally

[15]Present address: Vertex Pharmaceuticals Inc., San Diego, CA 92121, USA

[16]Lead Contact

*Correspondence: h.clevers@hubrecht.eu

https://doi.org/10.1016/j.cell.2017.11.010

## SUMMARY

Breast cancer (BC) comprises multiple distinct subtypes that differ genetically, pathologically, and clinically. Here, we describe a robust protocol for long-term culturing of human mammary epithelial organoids. Using this protocol, >100 primary and metastatic BC organoid lines were generated, broadly recapitulating the diversity of the disease. BC organoid morphologies typically matched the histopathology, hormone receptor status, and HER2 status of the original tumor. DNA copy number variations as well as sequence changes were consistent within tumor-organoid pairs and largely retained even after extended passaging. BC organoids furthermore populated all major gene-expression-based classification groups and allowed *in vitro* drug screens that were consistent with *in vivo* xeno-transplantations and patient response. This study describes a representative collection of well-characterized BC organoids available for cancer research and drug development, as well as a strategy to assess *in vitro* drug response in a personalized fashion.

## INTRODUCTION

Breast cancer (BC) is the most frequently diagnosed cancer and cause of cancer death among women worldwide (Stewart and Wild, 2014). BC comprises more than 20 distinct subtypes that differ genetically, morphologically, and clinically (Lakhani, 2012). BC heterogeneity is best exemplified by next-generation sequencing studies that have drawn comprehensive molecular BC portraits (Cancer Genome Atlas, 2012; Ciriello et al., 2015) and identified more than 1,600 likely driver mutations in 93 BC genes (Nik-Zainal et al., 2016). Despite the increased understanding of BC complexity, therapeutic approaches are currently largely based on clinical and pathological BC features, supplemented by hormone receptor and human epidermal growth factor receptor 2 (HER2) status (Lakhani, 2012). Consequently, the present standard systemic therapies (hormone, cytotoxic, and HER2-targeted) are unsatisfactorily tailored to individual patients. In response, rationally chosen targeted therapies are being evaluated in clinical trials (Zardavas et al., 2013), with individualized therapy being the final goal. Identifying unique molecular tumor features alone, however, can only guide treatment and will fail to predict clinical results without functional validation. Vice versa, functionally testing BC remedies *in vitro* could predict patient outcome even without molecular knowledge.

To functionally complement molecular and pathological BC analysis, representative and robust BC models are required

that can be generated efficiently. The most prevalent human-derived BC models to date are cell lines (Holliday and Speirs, 2011) and patient-derived xenografts (PDX) (Whittle et al., 2015). Although both model systems have contributed tremendously to translational BC research, they also have drawbacks (Vargo-Gogola and Rosen, 2007). Derivation of cell lines as well as PDXs is inefficient, labor-intensive, and requires multiple months per case, making it virtually impossible for them to contribute to individualized therapy on a broad scale. In addition, both models are usually derived from advanced-stage tumors and consequently do not fully capture the BC spectrum.

Inspired by three-dimensional cell culture systems of the mammary epithelium (Lee et al., 2007; Shaw et al., 2004), we established culture protocols that allow the generation and long-term expansion of three-dimensional epithelial organoids (Sato and Clevers, 2015; Sato et al., 2009). In contrast to the simultaneously developed culture method by Ootani et al. (2009), our adult stem cell-based cultures lack mesenchymal cells and generally require the following niche factors: the mitogen epidermal growth factor (EGF), the Wnt-agonist R-spondin, the transforming growth factor beta (TGF-β) inhibitor Noggin, and the extracellular matrix surrogate basement membrane extract (BME, or Matrigel). Depending on species and organ, additional common additives are among others (a.o.) Wnt-3A and fibroblast growth factor (FGF) 10, the activin receptor-like kinase (ALK) inhibitor A83-01, the p38 mitogen-activated protein kinase inhibitor SB202190, and the vitamin nicotinamide (Sato and Clevers, 2015). Organoids can be established from healthy as well as diseased donors (including cancer) and recapitulate the epithelial architecture and physiology of the organs they were isolated from (Clevers, 2016). We and others have successfully generated organoids from primary colon, prostate, and pancreatic cancers (Boj et al., 2015; Fujii et al., 2016; Gao et al., 2014; Sato et al., 2011; van de Wetering et al., 2015) and explored the potential advantages of organoid cultures in allowing functional tests and genotype-phenotype correlations (Neal and Kuo, 2016; Sachs and Clevers, 2014). Here, we describe efficient protocols for the culture of BC organoids and establish a representative collection of well-characterized BC organoids for BC research and drug discovery.

## RESULTS

### Establishing a Living BC Organoid Biobank

We obtained BC tissue from patients that underwent lumpectomy under informed consent (Table S1), removed normal tissue, and isolated BC cells through a combination of mechanical disruption and enzymatic digestion (see the STAR Methods). Isolated cells were plated in adherent BME drops and overlaid with optimized BC organoid culture medium (Figure 1A; Table S2). A key addition, compared to previously established human organoid protocols (Sato and Clevers, 2015; Sato et al., 2011), was the mitogen Neuregulin 1. Neuregulin 1 is a ligand of human EGF receptor (HER) tyrosine kinases -3 and -4 and has been implicated in mammary development as well as tumorigenesis (Roskoski, 2014; Troyer and Lee, 2001; Wansbury et al., 2008; Yang et al., 1995). Its addition to BC organoid medium allowed the efficient generation of BC organoids as well as their long-term expansion for >20 passages. Inhibition of Rho-associated coiled-coil containing protein kinase (ROCK) has been shown to allow long-term proliferation of tumor epithelial cells *in vitro* (Liu et al., 2012) and addition of the specific ROCK inhibitor Y-27632 indeed improved culture conditions. During medium optimization we furthermore noted that (1) addition of Wnt-3A did not improve culture conditions notably, (2) EGF concentrations above 5 ng × $ml^{-1}$ increased proliferation, but caused BC organoids to gradually sink through BME and lose their three-dimensional organization, and (3) SB202190 concentrations above 1 μM decreased efficiency of organoid establishment.

From 155 tumors, we established 95 BC organoid lines that readily expanded. Importantly, we did not observe a bias of organoid establishment with respect to histological subtype, grading, or receptor status of the original BC (Figure 1B; Table S1). Organoid lines could not always be established due to imperfect sampling and less effective earlier versions of the organoid medium. Following this learning-by-doing phase, we improved the success rate of BC organoid establishment to currently >80% and cryopreserved the majority of BC organoid lines (Table S1). While normal organoids consistently displayed a cystic phenotype, individual BC organoid lines differed greatly in their morphology as observed by bright-field microscopy. For example, we observed solid organoids of different sizes, cystic organoids, "grape-like" organoids, and organoids that were almost completely discohesive (Figure 1C; Movie S1). In order to generate a well-annotated living biobank as resource for academic research and drug discovery, we next set out to analyze BC organoids in depth by means of histology, whole genome DNA sequencing (WGS), RNA sequencing (RNA-seq), and drug testing (Figure 1D). In the following paragraphs, we describe the results of our ongoing effort to characterize the first set of BC organoids. All current and future BC organoid lines will be equally characterized, annotated, and made available on request as part of the HUB Living Biobank following approval by the internal review board of the University Medical Center Utrecht (METC-UMCU) (Figure 1D; see the STAR Methods).

### Histological Characterization of BC Organoids

For decades, BC has been classified into meaningful subgroups based on histological features (Azzopardi et al., 1979; Ellis et al., 1992; Elston and Ellis, 1991; Lakhani, 2012). Together with receptor status, histological grading and typing helps to describe distinct clinical presentations, suggest intervention strategies, and estimate survival rates (Lakhani, 2012). The most prevalent histological subtypes of BC are invasive ductal carcinoma of no special type (50%–80%) and invasive lobular carcinoma (5%–15%) (Lakhani, 2012). Our BC panel and derived BC organoids show a similar distribution (Figure 1B; Table S1). To test whether BC organoids match the original histological BC type, we performed blinded histopathological analysis of H&E stained tissue and organoid sections. The phenotype of BC organoid often agreed with the original BC (Figure 2; Table S3). For example, ductal carcinoma generally gave rise to solid, coherent organoids, while lobular carcinoma mainly generated discohesive organoids (Figure 2; Table S3). In addition, the majority of BC organoids was judged clearly malignant (Table S3) based on cellular and nuclear atypia. We, for example, regularly

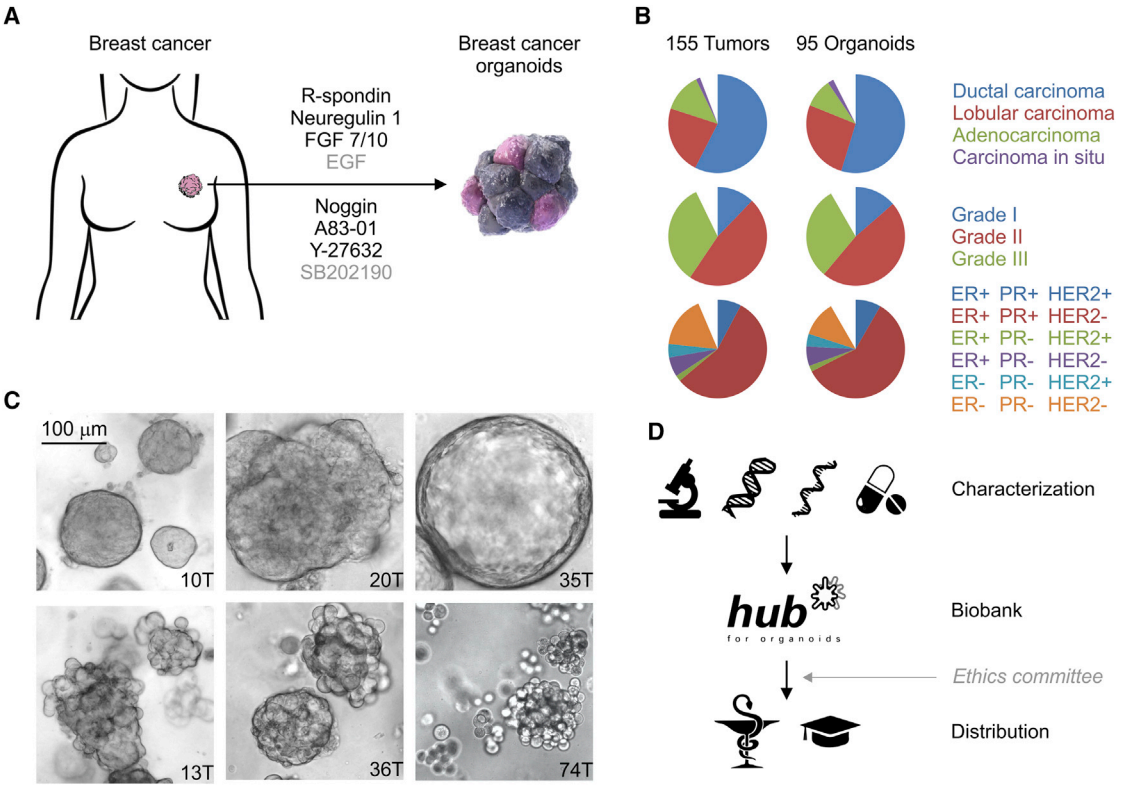


**Figure 1. Establishing a Biobank of BC Organoids**

(A) Diagram depicting the generation of BC organoid lines from primary BCs using optimized media components (black, essential components; gray, non-essential components, see Table S2).

(B) Pie charts comparing the stratification of all tumors with that of all derived organoid lines based on histological type (top), grade (middle), and receptor status (bottom). The composition of BC organoid lines is indistinguishable from that of the original tumors in all three categories, indicating that organoids can be established without bias from all BCs (see Table S1).

(C) Bright-field images depicting major BC organoid phenotypes. The top row shows cohesive organoids (left and middle: dense and solid; right: cystic and hollow), while the bottom row shows increasingly discohesive organoids (from left to right). Scale bar, 100 μm. See also Movie S1.

(D) Workflow summarizing the characterization of BC organoids by microscopy, DNA-sequencing, RNA-sequencing, and drug response, as well as their biobanking and subsequent distribution to academic or pharmaceutical third parties following ethical approval.

encountered typical cancerous features such as enlarged and polymorphic nuclei, high mitotic activity, apoptosis, and vacuole formation (signet ring cells) (Figure S1; Table S3). In contrast, control organoids established from histologically normal preventive mastectomy (PM) samples were very well organized and displayed only a mildly complex cribriform architecture (Figure S1) resembling benign ductal hyperplasia *in vivo*. PM organoids did not show cellular or nuclear atypia and were histologically judged to represent normal breast epithelium or ductal hyperplasia (Figure S1; Table S3).

Besides histological conservation, a representative BC model should retain expression of the most important and prevalent breast cancer biomarkers: estrogen receptor (ER), progesterone receptor (PR), and HER2. The status of hormone receptors ER and PR has predictive value for the outcome of hormone/endocrine BC therapy, while HER2 status can predict systemic chemotherapy outcome and in itself is a target for cancer therapies (Brennan and Lim, 2015; Dai et al., 2016). We indeed found hormone receptor and HER2 status to be maintained in the majority of BC tissue-organoid pairs as determined by immunohistochemistry. Tumors positive for ER and/or PR gave rise to ER- and/or PR-positive BC organoids in ~75% of cases. ER- and/or PR-negative tumors generated >90% ER- and/or PR-negative BC organoids. HER2 status was retained in 80% of HER2 positive and >90% of HER2 negative BC tissue-organoid pairs (Figures 2 and S1; Table S3).

In summary, we found that the majority of BC organoids matches the originating BC with respect to histopathology as well as hormone and HER2 receptor status. However, the histological analysis did not unequivocally assign tumor status to all BC organoids, with several lines being classified as either well-differentiated tumor or normal epithelium (Table S3). Thus, histological analysis can detect clear malignant morphological features of organoids from e.g., poorly differentiated tumors, yet it may fail to accurately categorize well-differentiated BC organoids, especially out of tissue-context.

## Genomic Characterization of BC Organoids

Whereas histological analysis benefits from stromal and inflammatory cells in tumor tissue, these cell populations impede

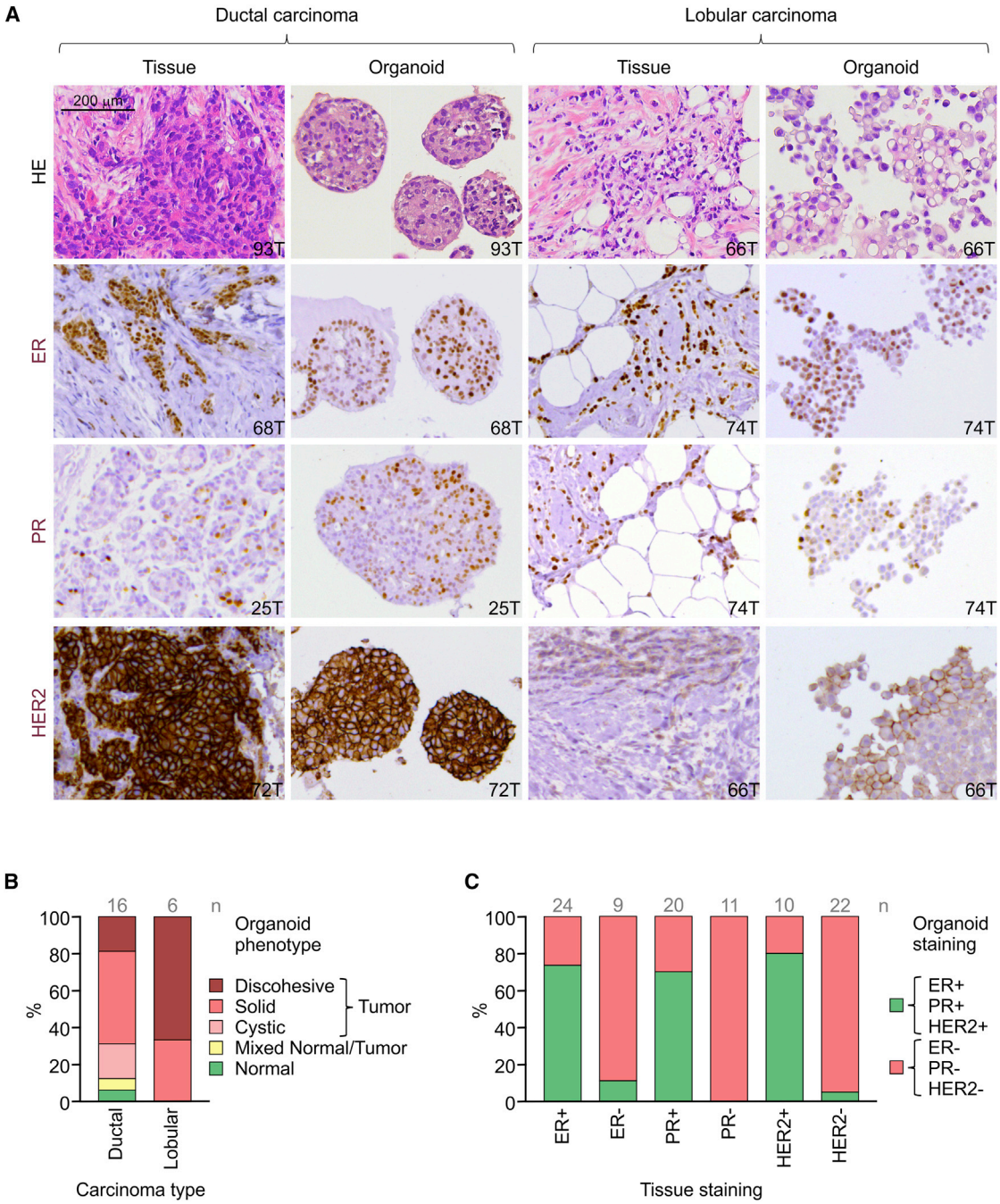


**Figure 2. Histology and Receptor Status of BC Organoids**

(A) Comparative histological and immunohistochemical images of BC and derived organoid lines. Shown are representative examples of ductal carcinoma (two columns on the left) and lobular carcinoma (two columns on the right). Tissues generally present tumor epithelium surrounded by mesenchymal and inflammatory cells, while organoids are exclusively epithelial with tumor cell organization being remarkably well conserved (HE). ER, PR, and HER2 status of original BCs are similarly well retained in the derived organoid lines. Scale bar, 200 µm. See Figure S1 for additional examples (DCIS, PM, TNBC) and high power magnifications of tumor cell details. See Table S3 for detailed histopathological analysis.

(B) Stacked bar chart showing the distribution of organoid phenotypes based on histopathological analysis grouped per original carcinoma type. Red colors indicate unequivocal characterization as pure tumor organoid (see also Table S3).

(C) Stacked bar chart showing the percentage of organoid lines that are receptor positive (green) and negative (red) grouped per original tumor receptor status (see also Table S3).

genomic analysis by masking genetic mutations. Vice versa, epithelial BC organoids represent the mutant cancer cells only. Since BC is often characterized by genetic instability and chromosomal imbalances (Danielsen et al., 2016), we first karyotyped BC organoids in order to verify their histologically assigned malignant status. We indeed found BC-characteristic chromosome number changes including frequent hyperdiploidies and occasional hypodiploidies (Figure 3A). We next employed WGS (STAR Methods) as current gold standard (Nik-Zainal et al., 2016) to characterize BC genomes including copy number alterations (CNAs) and somatic mutations. Per patient, we sequenced genomic DNA (gDNA) isolated from normal blood, BC tissue, and BC organoids (Figure S2A). In light of commonly misidentified and cross-contaminated cell lines (Lorsch et al., 2014), we first mapped genetic distances between all samples to verify the identity of each BC organoid line. Although the vast majority of patient-specific DNA samples indeed clustered together, we identified one case of swapped blood DNA samples as well as two cases of cross-contamination (Figure S2B), emphasizing the need for rigorous quality control. The latter cases were excluded from further analysis and additional organoid culture rules implemented to minimize future risk of cross-contamination (STAR Methods).

CNAs generally affect a large portion of the BC genome and include driver as well as passenger events (Pereira et al., 2016; Zack et al., 2013). Therefore, we first compared genome-wide CNAs of BCs and the corresponding BC organoids and as expected found multiple chromosome rearrangements including chromothripsis (Figure S3A; Table S3). DNA copy number gains and losses were retained throughout genomes (Figure 3B; Table S3) with BC organoids often showing much cleaner and more distinct copy number signals than original BCs. Importantly, these CNAs were largely retained even after extended passaging (Figure S3A). Next, we selected cancer genes exhibiting significant CNAs in breast cancer (Cancer Genome Atlas, 2012; Zack et al., 2013) and compared the respective CNA profiles of BCs with derived organoids. BC organoids recapitulated the original CNA patterns of cancer genes and generally showed a higher signal amplitude (Figure 3C) similarly to genome-wide CNAs (Figure 3B). Examples of specific BC genes whose CNAs were retained across several tumor-organoid pairs include *CDKN2A*, *ERBB2*, *NF1*, and *SNX31* (Figure 3C).

Cancers invariably accumulate somatic mutations that, depending on the affected gene(s), can drive cancer progression (Martincorena and Campbell, 2015). Driver as well as passenger mutations arise through diverse mutational processes resulting in distinct mutational signatures, at least 12 of which are found in BC (Alexandrov et al., 2013; Nik-Zainal et al., 2012, 2016). We mathematically analyzed base substitutions in BCs and organoids and plotted the total number of mutations per mutational signature per patient (Figure 4A). Not surprisingly, the total number of mutations as well as the relative contribution of individual signatures greatly differed between patients. For example, we found two hypermutated samples with more than 20,000 mutations. We furthermore identified significant contributions of all major BC signatures, including *kataegis* and BRCA-deficiency signatures (Figures 4A and 4B). In contrast to interpatient heterogeneity, mutation loads and types were mostly conserved in matching BC-organoid pairs (Figures 4A–4C; Table S4). Importantly, BC organoids displayed mutations in many of the most relevant BC genes (Banerji et al., 2012; Cancer Genome Atlas, 2012; Nik-Zainal et al., 2016; Pereira et al., 2016). For example, we found inactivating mutations in tumor suppressors *TP53* and *CDH1*, as well as *MLL2/3* epigenetic complexes and activating mutations in the oncogene *PIK3CA* (Figure 4D), most of which are conserved between BC-organoid pairs. In summary, we show that BC organoids recapitulate the diverse genomic landscape of BC including CNAs, mutational load and signatures, as well as cancer gene mutations.

## Gene Expression Analysis of BC Organoids and Gene Editing

Gene expression profiling contributed significantly to subcategorizing BC with several gene sets and analysis algorithms being used clinically (Schmidt et al., 2016). We therefore compared gene expression of normal and BC organoids by performing RNA-seq on 22 lines and assembling a correlation heatmap based on >25,000 genes. As shown in Figure 5A, normal organoids hierarchically clustered together with a subset of five BC organoid lines. The remaining 15 BC organoid lines clustered separately and were considerably more heterogeneous. When combining organoid expression data with >1,100 BC expression data from The Cancer Genome Atlas (TCGA) we found BC organoids to populate all major subclusters and distribute randomly throughout the dataset (Figure 5B). Multiple RNA expression-based BC classification systems have been proposed: PAM50, SCMGENE, SCMOD1, and IntClust (Ali et al., 2014; Desmedt et al., 2008; Haibe-Kains et al., 2012; Parker et al., 2009) with the first three classifiers mainly relating to receptor status. Organoids can be found in all subtypes with basal, luminal A, and normal subtypes dominating PAM50, and $ER^{-}/HER2^{-}$ and $HER^{+}$ subtypes dominating SCMGENE/SCMOD1 classifiers. IntClust, a 10 subtype classifier that additionally considers copy numbers, has organoids present in 7 subtypes with category iC4 containing most organoid lines. Subtype assignment reflects known subtype correspondence, namely iC10 with triple negative samples and iC5 with $HER2^{+}$. When comparing the expression profiles of discohesive versus solid BC organoids (Figure 2), we found expression differences in cell adhesion genes to be statistically overrepresented (Table S6). The resulting gene lists also included genes previously not implicated in BC cell adhesion (e.g., polymeric immunoglobulin receptor and protocadherins beta-16 and gamma b4). BC organoids therefore display representative gene expression profiles, which allow hierarchical clustering into the majority of RNA expression-based BC subtypes without a significant culture bias, and aid the characterization of epithelial cell biological phenomena. To test if mammary gland organoids can be experimentally manipulated, we generated functional *TP53* mutant clones through CRISPR/Cas9-mediated gene editing (Figure S4).

## Drug Screen

In order to evaluate BC organoids as functional *in vitro* disease models, we tested whether BC organoids could be used for high-throughput drug sensitivity screens. We chose a small set of drugs targeting the HER signaling pathway (Figure 6A) and

Please cite this article in press as: Sachs et al., A Living Biobank of Breast Cancer Organoids Captures Disease Heterogeneity, Cell (2018), https://doi.org/10.1016/j.cell.2017.11.010



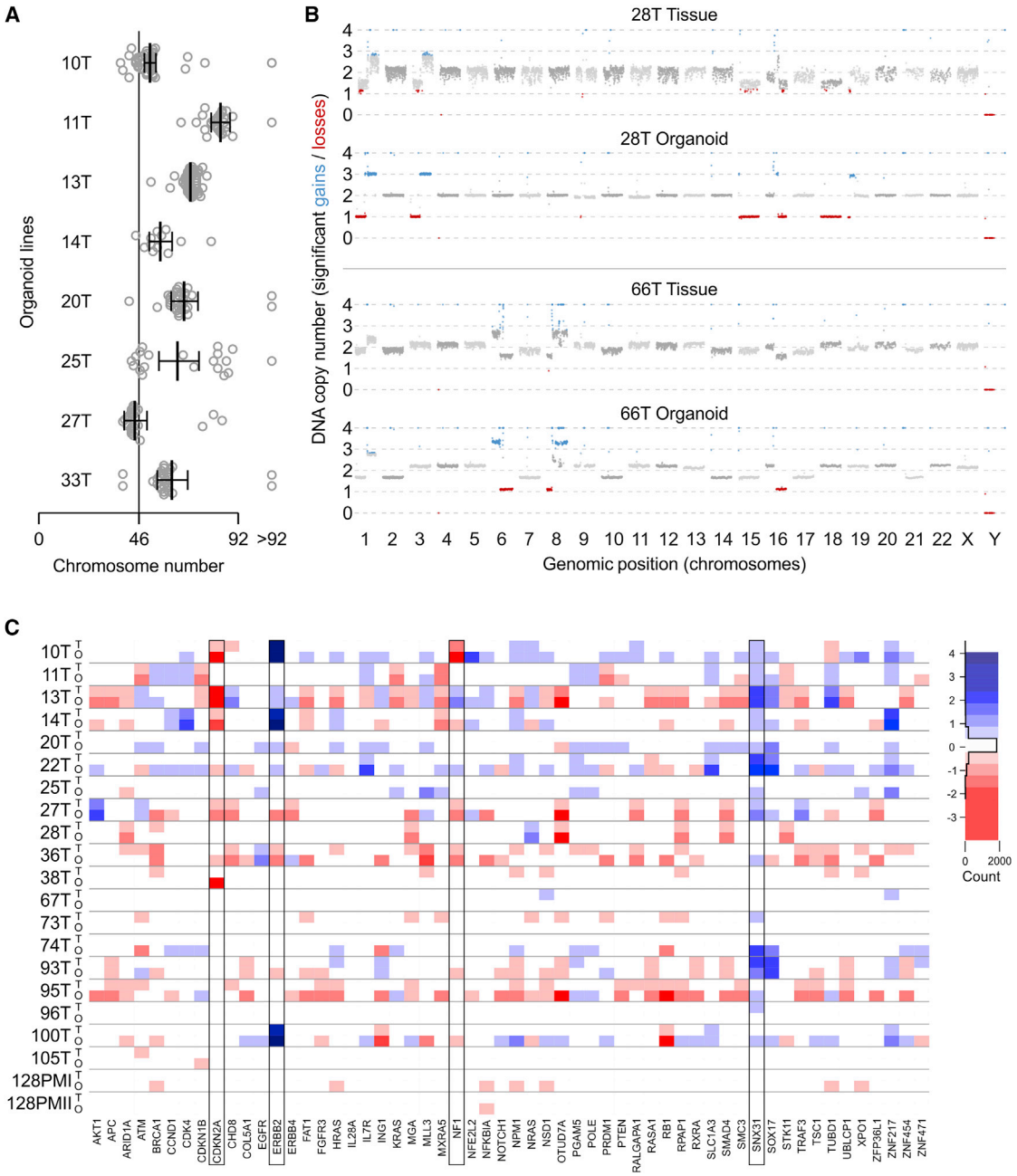


**Figure 3. Copy Number Alterations of BC Organoids**

(A) Box-and-whisker plot showing karyotypes of BC organoid lines with several degrees of aneuploidy. For example, 10T and 27T show mildly abnormal chromosome numbers whereas those of 11T and 13T are substantially higher. 25T shows a bimodal distribution near-diploid as well as near-tetraploid.

(B) Scatterplots illustrating genome wide CNAs of BC tissue-organoid pairs. DNA copy number gains (blue) and losses (red) found in the original BC are conserved in the derived organoid lines. Note the increased resolution and signal amplification in epithelial organoids compared to mixed tumor tissue. See also Figures S2 and S3A and Tables S3 and S4.

(C) Heatmap showing CNAs in coding DNA sequences of BC genes (see STAR Methods). Copy numbers are plotted as $\log_2$-transformed ratios per gene and grouped per patient (T, tissue; O, organoid). Selected cancer genes are highlighted by boxes showing conserved copy number gains (blue) or losses (red) among BC-organoid pairs. Note the near absence of CNAs in PM samples.

performed cell viability assays as described for colorectal cancer (CRC) organoids (van de Wetering et al., 2015). Using 21 concentrations per drug we were able to generate reproducible dose-response curves and identify half-maximal inhibitory concentrations ($IC_{50}$) (Figures 6B and 6C). In the majority of cases, we found a homogeneous response to a certain drug yielding

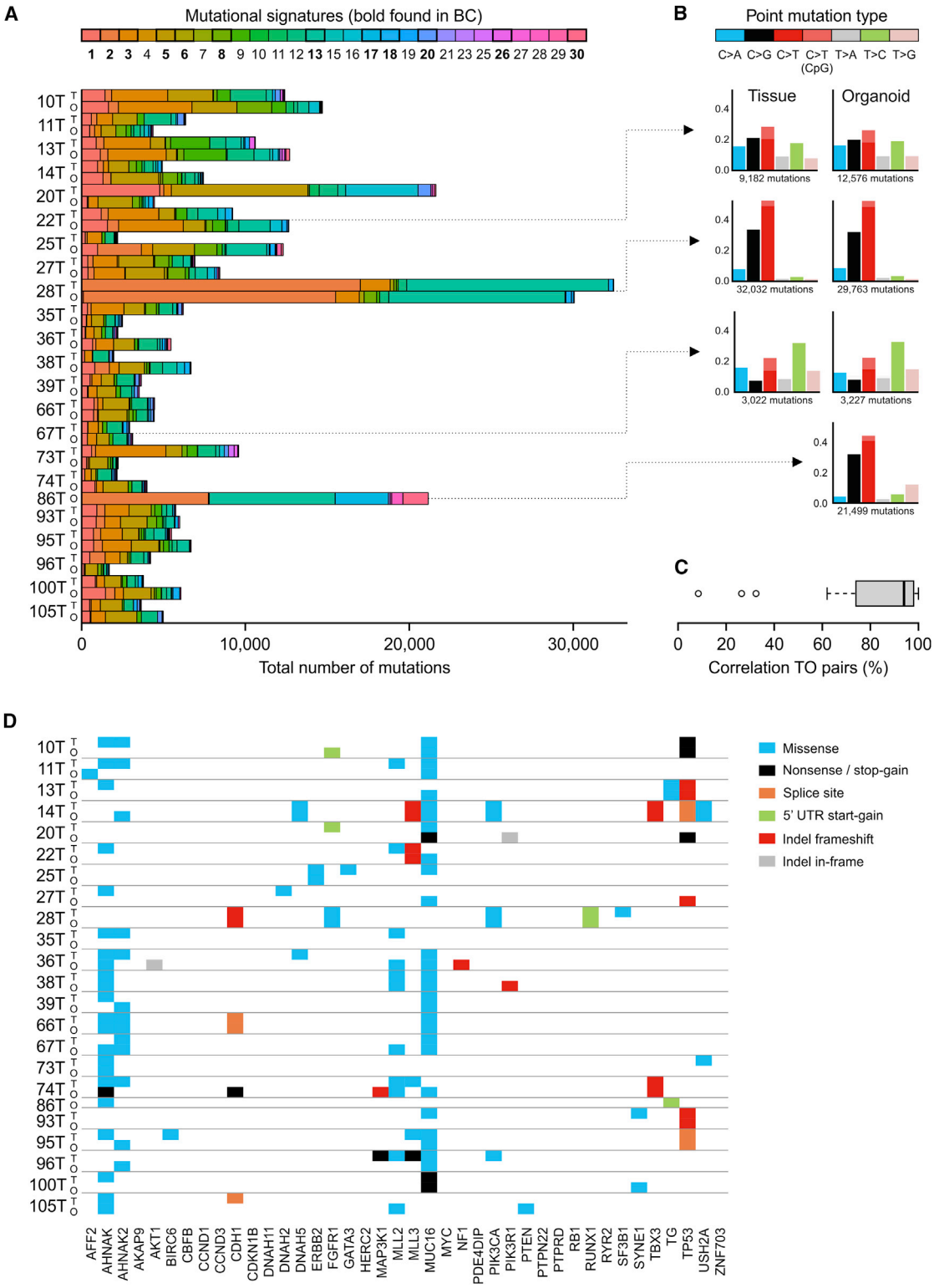


**Figure 4. Mutational Signatures and Driver Gene Analysis**

(A) Stacked bar graphs showing the total mutation load per mutational signature per patient sample pair (T, tissue; O, organoid). Typical BC mutational signatures (bold) are present and conserved between corresponding tissue and organoid samples (see also Figure 4C and Table S4). 28T and 86T show >20,000 mutations mainly belonging to signatures 2 and 13, which are commonly found in locally hypermutated BCs (*kataegis*) and associated with AID/APOBEC enzymes.

*(legend continued on next page)*

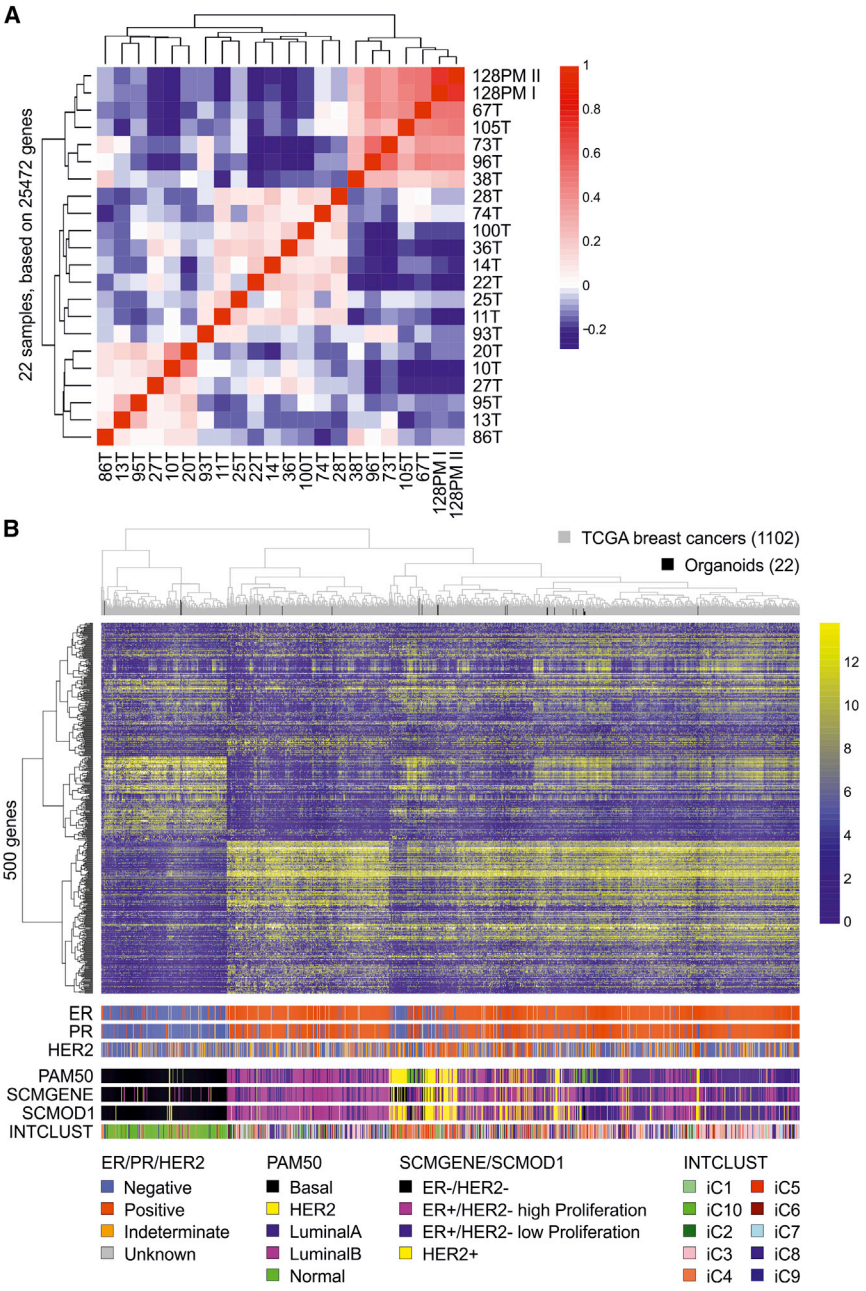


**Figure 5. Gene Expression Analysis of BC Organoids by RNA-Seq**

(A) Correlation heatmap of BC organoids and organoids derived from preventive mastectomies (128 PM I and II). The 22 organoid RNA-seq samples were normalized for sequencing depth (see STAR Methods), $\log_2$-transformed, and mean-centered by genes (rows). Spearman correlations were calculated for all sample-pairs, using all 25,991 genes. The heatmap shows clustering of samples by 1-correlation distance using complete linkage for hierarchical clustering. Cells are color-coded by the Spearman correlation value.

(B) Organoid RNA-seq data (22 samples) was normalized and combined with TCGA RNA-seq data (1,102 samples, see STAR Methods). The combined data were clustered using the 500 most varying genes using 1-correlation distance with complete linkage. The distribution of organoid samples among TCGA data is indicated by black lines. Annotation rows show ER, PR, and HER2 status determined by staining, followed by subtype assignments according to PAM50, SCMGENE, SCMOD1, and IntClust classifiers (for details see Table S5).

a single $IC_{50}$. However, we sometimes found several relative $IC_{50}$ values, indicating the presence of differentially susceptible organoid subpopulations (Figure 6B). Overall, organoids were sensitive to drugs blocking the HER signaling pathway, when they overexpressed HER2 and drug-resistant in the absence of HER2. However, a few organoid lines defied these expectations (Figure 6B), emphasizing the value of functional *in vitro* drug tests on BC organoids. Poly(ADP-ribose)polymerase inhibitors (PARPis) are successfully being used in BC patients with defective BRCA-mediated genome repair pathways (Lee et al., 2014). We subjected BC organoid lines with the highest and lowest relative contributions of mutant BRCA1/2 signatures to increasing concentrations of the PARPis olaparib and niraparib and assessed cell viability as above. While BC organoids with high BRCA1/2 signatures were sensitive to PARPi, BC organoids with low BRCA1/2 signatures were not (Figure 6C). Of note, line 10T did not show BRCA1/2 mutations despite high BRCA1/2 signatures, highlighting the advantage of WGS in combination with functional drug screens on BC organoids.

Signature 3, which is strongly associated with *BRCA1* and *BRCA2* mutations, accounts for a high percentage of mutations in multiple samples including 10T, 13T, 22T, and 27T.

(B) Bar graphs showing the relative contributions of point mutation types underlying mutational signatures for selected cases. Mutation types differ greatly between patients, but are conserved among matching tissue/organoid pairs.

(C) Box-and-whisker plot showing the correlation percentages of mutational spectra of tissue/organoid pairs (see also Table S4).

(D) Overview of somatic mutations found in BC genes of BC-organoid pairs grouped per patient (T, tissue; O, organoid). Shown is the most severe mutation per gene, examples include missense mutations (e.g., *AHNAK*, *MLL2*, and *MUC16*) and nonsense, splice site mutations as well as frameshift indels (e.g., *CDH1* and *TP53*).

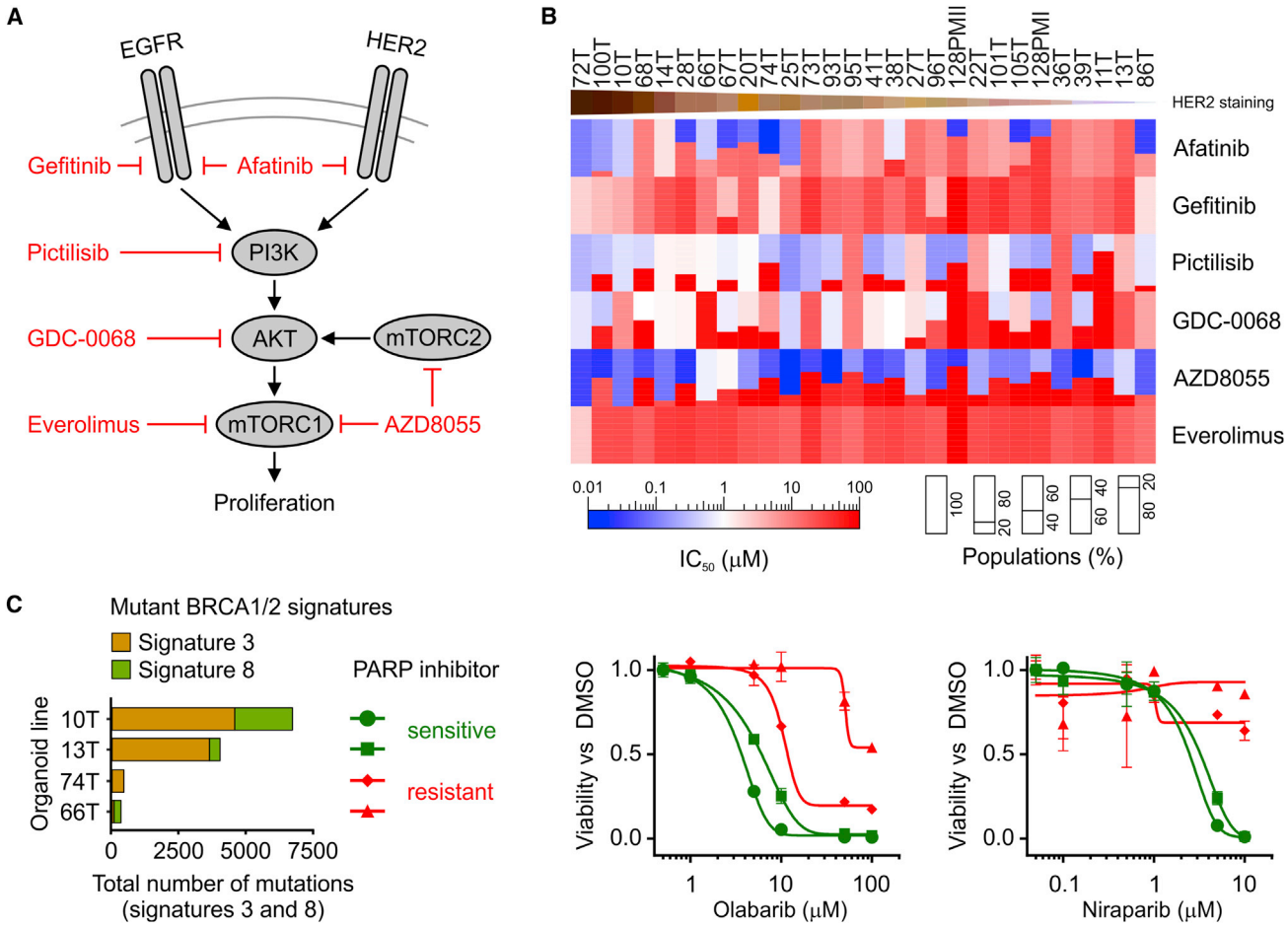


**Figure 6. BC Organoids Allow *In Vitro* Drug Screening**

(A) Simplified scheme of the HER signaling pathway including used drugs.

(B) Heat-map of $IC_{50}$ values of six drugs targeting the HER signaling pathway in 28 organoid lines sorted by HER2 staining intensity. Where organoids showed multiple relative $IC_{50}$ values, the respectively contributing percentages are indicated. As expected, most HER2-overexpressing organoids are sensitive to drugs targeting the HER signaling pathway, while HER2-negative organoids are resistant. Notable exceptions are 68T (HER2 positive) and 86T (HER2 negative).

(C) The left bar graph plots the total number of BRCA1/2 signature mutations of BC organoids 10T and 13T (highest) and 74T and 66T (lowest). Their predicted response to PARPi is indicated in green (sensitive) and red (resistant). The dose-response curves on the right indicate BC organoid viabilities after 2 weeks in the presence of increasing concentrations of the PARPis olaparib and niraparib. Functional responses to both PARPis match the genomically predicted ones. Error bars represent SEM of two to three independent experiments.

## Comparison to Drug Response *In Vivo*

To compare *in vitro* with *in vivo* drug responses, we first selected two BC organoid lines that responded differently to drugs blocking HER signaling *in vitro* (Figure 7A) and transplanted each line orthotopically into both flanks of 10 mice. Once a tumor grew larger than 50 $mm^3$, the respective mouse was either treated with 10 μg/g bodyweight afatinib or with vehicle for 28 days (Figure 7B). Tumors originating from afatinib-resistant BC organoid line 27T grew at virtually the same rates when treated with afatinib or vehicle (Figure 7B). In contrast, tumors originating from afatinib-sensitive line 10T grew significantly slower when treated with afatinib compared to vehicle (Figure 7B). Consequently, mice carrying 27T tumors had to be sacrificed at the same time irrespective of treatment type, while mice carrying 10T tumors lived significantly longer when given afatinib compared to vehicle (Figure 7B) recapitulating the respective *in vitro* drug response. Because the established BC organoid lines were derived from surgically removed BCs, we were unable to correlate *in vitro* drug response directly to patient responses. We therefore generated 12 BC organoid lines from needle biopsies of 13 patients with metastatic BC (Table S1). Patients were given standard of care treatment and responses recorded (Table S1). Tamoxifen was the only drug that resulted in differential responses in our limited metastatic BC set (Table S1) with one patient being responsive, one non-responsive, and the remainder undetermined. *In vitro* responses of the BC organoids to tamoxifen matched that of the respective patients (Figure 7C) indicating the potential use of BC organoids as predictive *in vitro* surrogates for BC *in vivo*.

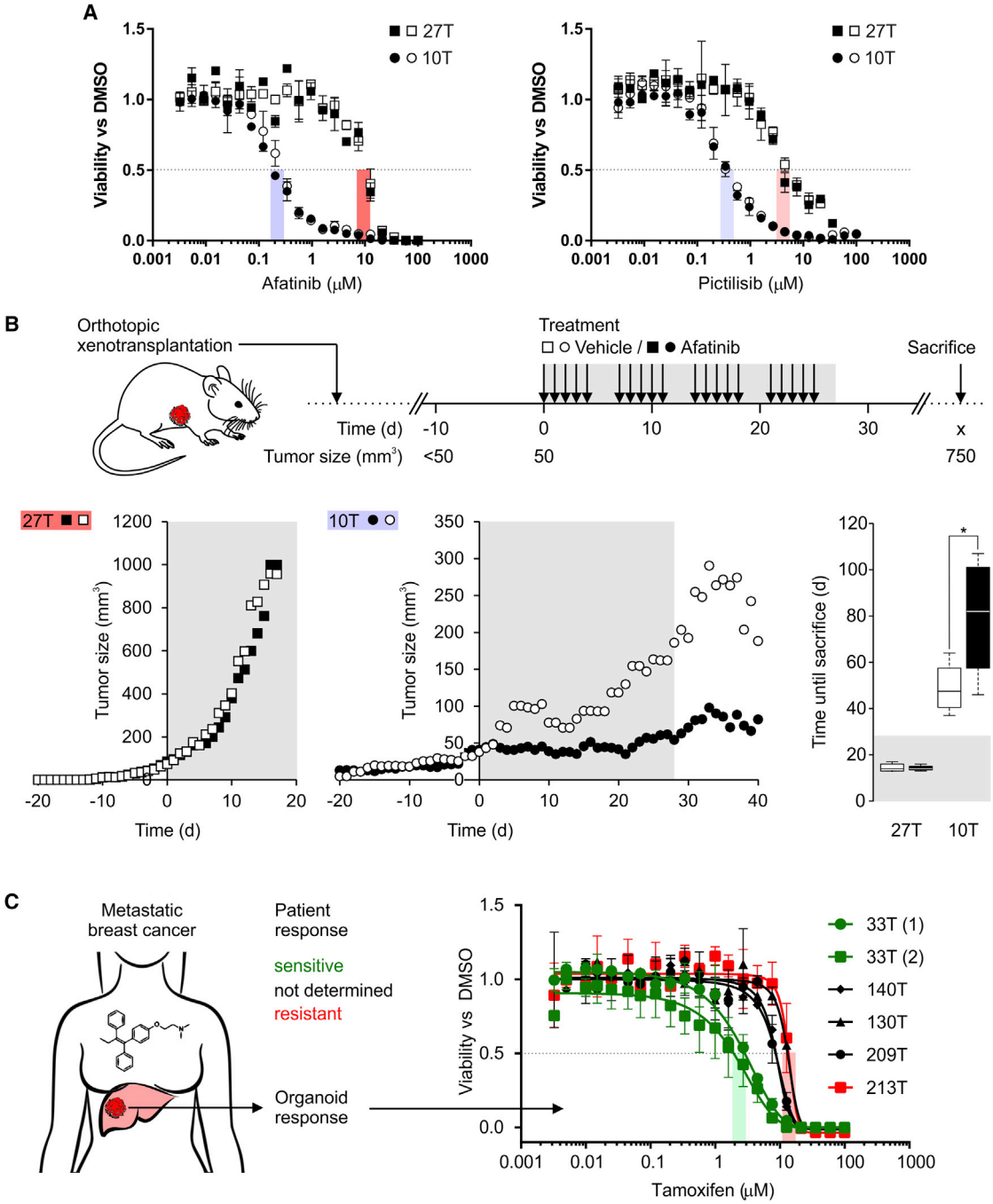


**Figure 7. BC Organoids Recapitulate *In Vivo* Drug Responses**

(A) Dose-response curves of afatinib and pictilisib of HER2-overexpressing line 10T and HER2-negative line 27T of two independent experiments. $IC_{50}$ values are indicated using the color-scheme of (Figure 6B). Error bars represent SD of technical duplicates.

(B) Top: Schematic of targeting the HER signaling pathway *in vivo*. Mice were orthotopically transplanted with BC organoids and treated for the indicated period as soon as tumor volumes reached 50 $mm^3$. Mice were sacrificed when the tumors exceeded 500 $mm^3$. Bottom: Averaged HER2-negative 27T and HER2-overexpressing 10T tumor volumes over time. Black data points indicate afatinib-treated mice, white data points indicate vehicle controls. While 27T tumors do not differ, 10T tumors on afatinib-treated mice grow much slower with mice dying significantly later than vehicle controls (n = 5 mice per group, *…$p < 0.05$ t test). Error bars represent SEM of five to six independently injected mice.

(C) Schematic drawing indicating the experimental set-up of generating organoid lines from metastatic BC patients. Patient response to standard of care treatment (here tamoxifen) is recorded (see also Table S1) and compared to *in vitro* response of the respectively derived BC organoids (dose-response curve on

*(legend continued on next page)*

In summary, BC organoids can be generated efficiently from all major BC subtypes. BC organoids capture and retain histological as well as genetic BC heterogeneity and allow physiologically relevant *in vitro* drug screens.

## DISCUSSION

For decades, pre-clinical BC research has relied on a few dozens of cell lines as *in vitro* representations of a heterogeneous disease affecting millions of patients. While amenable to high-throughput screening, BC cell lines do not fully capture the BC spectrum and are rarely of clinical relevance for individual patients (Sharma et al., 2010). PDX models, as the other pillar of pre-clinical BC research, capture tumor heterogeneity, but traditionally have not allowed for high-throughput screening. Recently, several groups tackled this problem by directly treating mice *in vivo* (Gao et al., 2015) or PDX-derived cultures *in vitro* (Bruna et al., 2016). Although very promising, both methods still depend on inefficient PDX generation and the latter does not allow extended passaging *in vitro*.

By adapting previously published organoid protocols (Sato and Clevers, 2015), we overcame both hurdles with the addition of Neuregulin 1 allowing both the efficient generation and long-term maintenance of BC organoids. Because BC organoids recapitulate central BC features, they may represent a third pre-clinical BC model in between 2D cell lines *in vitro* and PDX models *in vivo*. The first striking feature of BC organoids is their phenotypic diversity that appears to reflect BC histology: while ductal BCs usually give rise to solid organoids, lobular BCs most often generate discohesive organoids. Lobular histology appears to correlate with poor survival when adjusted for other patient parameters (Korhonen et al., 2013). Discohesive BC organoids could be a unique experimental tool to better understand the underlying mechanisms of lobular histology and identify potential drug targets. While we, for example, identify loss of E-cadherin function in a subset of discohesive BC organoids (28T, 66T, and 74T) as expected (Christgen et al., 2016), other organoids await a molecular explanation. Because mammary gland organoids lend themselves to gene editing, phenotypic screens can easily be performed and hypotheses tested. The second central feature of BC organoids is the advantage to extract genetic data from pure tumor epithelium. The absence of ''contaminating'' genetically normal cell types allows for much cleaner CNA profiles as well as easier detection of somatic mutations. The same holds true for gene expression analysis, where expression-based subtypes could clearly be assigned to the majority of BC organoids and the cause of biological phenomena such as epithelial cell adhesion be interrogated. However, the absent tumor environment *in vitro* may cause differences between expression profiles of tumor-organoid pairs (Soysal et al., 2015). The respective correlation analysis is currently missing, because tumor RNA was not collected following BC resection in the current study. Future studies, where tumor RNA collection is practically implemented, should shed light on this issue and may dissect the influence of the tumor environment on gene expression of cancer cells and vice versa.

The third critical feature of BC organoids is the possibility to perform functional high-throughput drug screens, as demonstrated earlier for CRC organoids (van de Wetering et al., 2015). Importantly, drug sensitivities obtained *in vitro* appear to bear physiological significance as shown here in proof of concept xeno-transplantation assays and recapitulation of the tamoxifen response of metastatic BC patients by derived BC organoid lines. In order to unequivocally translate these findings, organoids should be generated from BC biopsies and treated in parallel to the respective patients in defined clinical trials. Ideally, BC organoids could aid in identifying possible treatment strategies and resistances for individual patients even in the absence of molecular underpinnings. Indeed, CRC organoid drug screens have recently been used to functionally identify resistance mechanisms of targeted therapies (Verissimo et al., 2016). Correlating histological, genetic, and/or gene expression data to BC organoid drug responses will further advance our molecular and functional understanding of BC.

In order to share established BC organoid lines and relevant data ethically responsibly with the scientific community, while protecting patient confidentiality and the right to withdraw informed consent, HUB and METC-UMCU implemented a rigorous protocol overseeing biobanking and case-by-case distribution. We already built a living biobank of more than 100 BC organoid lines from a wide variety of primary and metastatic tumors without bias and will continue to do so until we reached a comprehensive BC organoid set representative of all BC subtypes. In conclusion, we propose BC organoids as valuable pre-clinical BC model for academic, clinical, and pharmaceutical research.

## STAR★METHODS

Detailed methods are provided in the online version of this paper and include the following:

- KEY RESOURCE TABLE
- CONTACT FOR REAGENT AND RESOURCE SHARING
- EXPERIMENTAL MODELS AND SUBJECT DETAILS
  - Approval of studies involving humans and patient informed consent
  - BC tissue processing
  - BC organoid culture
  - Xeno-transplantations
- METHOD DETAILS
  - Histology and imaging
  - Genomic analysis
  - RNA-seq analysis

the right). The tamoxifen-sensitive BC metastasis gave rise to a tamoxifen-sensitive organoid line (green), while the tamoxifen resistant metastasis gave rise to a tamoxifen resistant organoid line (red). Patients that were not given tamoxifen as standard of care ( = patient response not determined) were most likely considered to be non-responsive explaining their tamoxifen-resistant phenotype *in vitro* (black). Error bars represent SEM of two to three independent experiments.

## SUPPLEMENTAL INFORMATION

Supplemental Information includes four figures, six tables, and one movie and can be found with this article online at https://doi.org/10.1016/j.cell.2017.11.010.

## AUTHOR CONTRIBUTIONS

Conceptualization, N.S., R.G.J.V., E.C., and H.C.; Methodology, N.S., J.d.L., O.K., R.v.B., L.W., E.C., and H.C.; Software, J.d.L., G.B., A.v.H., R.v.B., F.B., R.F.E., I.J.N., M.H., L.W.; Formal Analysis, N.S., J.d.L., O.K., G.B., A.v.H., R.v.B., L.W., P.J.v.D., E.C.; Investigation, N.S., J.d.L., O.K., E.G., G.B., F.W., A.V.B., K.W., A.G., H.B., J.K., A.A.D., D.L., and P.J.v.D.; Data Curation, J.d.L.; Writing – Original Draft, N.S. and H.C.; Visualization, N.S., J.d.L., A.v.H., and G.B.; Supervision, M.v.d.V., D.A.E., S.F.B., E.E.V., L.W., S.R., R.G.J.V., E.C., and H.C.; Project Administration, N.S., V.Z., J.M., S.F.B., R.G.J.V., E.C., and H.C.; Funding Acquisition, N.S., V.Z., J.M., E.E.V., L.W., S.R., R.G.J.V., E.C., and H.C.

## ACKNOWLEDGMENTS

We thank all patients participating in this study as well as the teams approaching patients for consent and collecting tissue. We thank Tulay Bayram for supporting regulatory affairs. We acknowledge the Hubrecht Imaging Center for providing imaging support. We thank the Utrecht Sequencing Facility (USF) for providing the sequencing data and service. USF is subsidized by the Hubrecht Institute, Utrecht University, and the UMC Utrecht Center for Molecular Medicine. This work was funded by MKMD grant 114021012 and grants from the Netherlands Organization for Scientific Research (NWO-ZonMw 91615182 and 114021012), a Stand Up to Cancer International Translational Cancer Research Grant (a program of the Entertainment Industry Foundation administered by the AACR), Stichting Vrienden van Hubrecht (2012.010), the Cancer Genomic Center, Pink Ribbon (grant 2014-186), and Boehringer-Ingelheim RCV GmbH & Co KG (contract 141947). N.S., A.G., S.F.B., and H.C. are inventors on patent applications/patents for organoid culture. S.F.B. and R.G.J.V. are full-time employees of the Foundation Hubrecht Organoid Technology (HUB), which holds the exclusive license of organoid technology patents. V.Z. and J.M. are full-time employees of Boehringer-Ingelheim RCV GmbH & Co KG. This work was supported in part by Boehringer Ingelheim RCV GmbH & Co KG.

Received: November 20, 2016
Revised: October 6, 2017
Accepted: November 3, 2017
Published: December 7, 2017

## REFERENCES

Alexandrov, L.B., Nik-Zainal, S., Wedge, D.C., Aparicio, S.A., Behjati, S., Biankin, A.V., Bignell, G.R., Bolli, N., Borg, A., Børresen-Dale, A.L., et al.; Australian Pancreatic Cancer Genome Initiative; ICGC Breast Cancer Consortium; ICGC MMML-Seq Consortium; ICGC PedBrain (2013). Signatures of mutational processes in human cancer. Nature *500*, 415–421.

Ali, H.R., Rueda, O.M., Chin, S.F., Curtis, C., Dunning, M.J., Aparicio, S.A., and Caldas, C. (2014). Genome-driven integrated classification of breast cancer validated in over 7,500 samples. Genome Biol. *15*, 431.

Anders, S., Pyl, P.T., and Huber, W. (2015). HTSeq–a Python framework to work with high-throughput sequencing data. Bioinformatics *31*, 166–169.

Azzopardi, J.G., Ahmed, A., and Millis, R.R. (1979). Problems in breast pathology. Major Probl. Pathol. *11*, i–xvi, 1–466.

Banerji, S., Cibulskis, K., Rangel-Escareno, C., Brown, K.K., Carter, S.L., Frederick, A.M., Lawrence, M.S., Sivachenko, A.Y., Sougnez, C., Zou, L., et al. (2012). Sequence analysis of mutations and translocations across breast cancer subtypes. Nature *486*, 405–409.

Blokzijl, F., de Ligt, J., Jager, M., Sasselli, V., Roerink, S., Sasaki, N., Huch, M., Boymans, S., Kuijk, E., Prins, P., et al. (2016a). Tissue-specific mutation accumulation in human adult stem cells during life. Nature *538*, 260–264.

Blokzijl, F., Janssen, R., Van Boxtel, R., and Cuppen, E. (2016b). MutationalPatterns: an integrative R package for studying patterns in base substitution catalogues. bioRxiv. Published online October 17, 2017. https://doi.org/10.1101/071761.

Boeva, V., Popova, T., Bleakley, K., Chiche, P., Cappo, J., Schleiermacher, G., Janoueix-Lerosey, I., Delattre, O., and Barillot, E. (2012). Control-FREEC: a tool for assessing copy number and allelic content using next-generation sequencing data. Bioinformatics *28*, 423–425.

Boj, S.F., Hwang, C.I., Baker, L.A., Chio, I.I., Engle, D.D., Corbo, V., Jager, M., Ponz-Sarvise, M., Tiriac, H., Spector, M.S., et al. (2015). Organoid models of human and mouse ductal pancreatic cancer. Cell *160*, 324–338.

Borst-Eilers, E., and Sorgdrager, W. (1998). Wet medisch-wetenschappelijk onderzoek met mensen. http://wetten.overheid.nl/BWBR0009408/2016-08-01.

Brennan, M., and Lim, B. (2015). The actual role of receptors as cancer markers, biochemical and clinical aspects: receptors in breast cancer. Adv. Exp. Med. Biol. *867*, 327–337.

Bruna, A., Rueda, O.M., Greenwood, W., Batra, A.S., Callari, M., Batra, R.N., Pogrebniak, K., Sandoval, J., Cassidy, J.W., Tufegdzic-Vidakovic, A., et al. (2016). A biobank of breast cancer explants with preserved intra-tumor heterogeneity to screen anticancer compounds. Cell *167*, 260–274.

Cancer Genome Atlas, N.; Cancer Genome Atlas Network (2012). Comprehensive molecular portraits of human breast tumours. Nature *490*, 61–70.

Christgen, M., Steinemann, D., Kühnle, E., Länger, F., Gluz, O., Harbeck, N., and Kreipe, H. (2016). Lobular breast cancer: Clinical, molecular and morphological characteristics. Pathol. Res. Pract. *212*, 583–597.

Cibulskis, K., Lawrence, M.S., Carter, S.L., Sivachenko, A., Jaffe, D., Sougnez, C., Gabriel, S., Meyerson, M., Lander, E.S., and Getz, G. (2013). Sensitive detection of somatic point mutations in impure and heterogeneous cancer samples. Nat. Biotechnol. *31*, 213–219.

Cingolani, P., Platts, A., Wang, L., Coon, M., Nguyen, T., Wang, L., Land, S.J., Lu, X., and Ruden, D.M. (2012). A program for annotating and predicting the effects of single nucleotide polymorphisms, SnpEff: SNPs in the genome of Drosophila melanogaster strain w1118; iso-2; iso-3. Fly (Austin) *6*, 80–92.

Ciriello, G., Gatza, M.L., Beck, A.H., Wilkerson, M.D., Rhie, S.K., Pastore, A., Zhang, H., McLellan, M., Yau, C., Kandoth, C., et al.; TCGA Research Network (2015). Comprehensive molecular portraits of invasive lobular breast cancer. Cell *163*, 506–519.

Clevers, H. (2016). Modeling development and disease with organoids. Cell *165*, 1586–1597.

Dai, X., Xiang, L., Li, T., and Bai, Z. (2016). Cancer hallmarks, biomarkers and breast cancer molecular subtypes. J. Cancer *7*, 1281–1294.

Danielsen, H.E., Pradhan, M., and Novelli, M. (2016). Revisiting tumour aneuploidy - the place of ploidy assessment in the molecular era. Nat. Rev. Clin. Oncol. *13*, 291–304.

Desmedt, C., Haibe-Kains, B., Wirapati, P., Buyse, M., Larsimont, D., Bontempi, G., Delorenzi, M., Piccart, M., and Sotiriou, C. (2008). Biological processes associated with breast cancer clinical outcome depend on the molecular subtypes. Clin. Cancer Res. *14*, 5158–5165.

Dobin, A., Davis, C.A., Schlesinger, F., Drenkow, J., Zaleski, C., Jha, S., Batut, P., Chaisson, M., and Gingeras, T.R. (2013). STAR: ultrafast universal RNA-seq aligner. Bioinformatics *29*, 12–21.

Drost, J., van Jaarsveld, R.H., Ponsioen, B., Zimberlin, C., van Boxtel, R., Buijs, A., Sachs, N., Overmeer, R.M., Offerhaus, G.J., Begthel, H., et al. (2015). Sequential cancer mutations in cultured human intestinal stem cells. Nature *521*, 43–47.

Durinck, S., Spellman, P.T., Birney, E., and Huber, W. (2009). Mapping identifiers for the integration of genomic datasets with the R/Bioconductor package biomaRt. Nat. Protoc. *4*, 1184–1191.

Ellis, I.O., Galea, M., Broughton, N., Locker, A., Blamey, R.W., and Elston, C.W. (1992). Pathological prognostic factors in breast cancer. II. Histological type. Relationship with survival in a large study with long-term follow-up. Histopathology *20*, 479–489.

Elston, C.W., and Ellis, I.O. (1991). Pathological prognostic factors in breast cancer. I. The value of histological grade in breast cancer: experience from a large study with long-term follow-up. Histopathology *19*, 403–410.

Ethik Kommission Ärztekammer Hamburg (2015). Sonstige Studien - Ärztekammer Hamburg. https://www.aerztekammer-hamburg.org/sonstige_studien.html.

Fujii, M., Shimokawa, M., Date, S., Takano, A., Matano, M., Nanki, K., Ohta, Y., Toshimitsu, K., Nakazato, Y., Kawasaki, K., et al. (2016). A colorectal tumor organoid library demonstrates progressive loss of niche factor requirements during tumorigenesis. Cell Stem Cell *18*, 827–838.

Gao, D., Vela, I., Sboner, A., Iaquinta, P.J., Karthaus, W.R., Gopalan, A., Dowling, C., Wanjala, J.N., Undvall, E.A., Arora, V.K., et al. (2014). Organoid cultures derived from patients with advanced prostate cancer. Cell *159*, 176–187.

Gao, H., Korn, J.M., Ferretti, S., Monahan, J.E., Wang, Y., Singh, M., Zhang, C., Schnell, C., Yang, G., Zhang, Y., et al. (2015). High-throughput screening using patient-derived tumor xenografts to predict clinical trial drug response. Nat. Med. *21*, 1318–1325.

Garrison, E., and Marth, G. (2012). Haplotype-based variant detection from short-read sequencing. arXiv: 1207.3907.

Gendoo, D.M., Ratanasirigulchai, N., Schröder, M.S., Paré, L., Parker, J.S., Prat, A., and Haibe-Kains, B. (2016). Genefu: an R/Bioconductor package for computation of gene expression-based signatures in breast cancer. Bioinformatics *32*, 1097–1099.

Haibe-Kains, B., Desmedt, C., Loi, S., Culhane, A.C., Bontempi, G., Quackenbush, J., and Sotiriou, C. (2012). A three-gene model to robustly identify breast cancer molecular subtypes. J. Natl. Cancer Inst. *104*, 311–325.

Holliday, D.L., and Speirs, V. (2011). Choosing the right cell line for breast cancer research. Breast Cancer Res. *13*, 215.

Johnson, W.E., Li, C., and Rabinovic, A. (2007). Adjusting batch effects in microarray expression data using empirical Bayes methods. Biostatistics *8*, 118–127.

Koboldt, D.C., Zhang, Q., Larson, D.E., Shen, D., McLellan, M.D., Lin, L., Miller, C.A., Mardis, E.R., Ding, L., and Wilson, R.K. (2012). VarScan 2: somatic mutation and copy number alteration discovery in cancer by exome sequencing. Genome Res. *22*, 568–576.

Korhonen, T., Kuukasjärvi, T., Huhtala, H., Alarmo, E.L., Holli, K., Kallioniemi, A., and Pylkkänen, L. (2013). The impact of lobular and ductal breast cancer histology on the metastatic behavior and long term survival of breast cancer patients. Breast *22*, 1119–1124.

Lakhani, S.R. (2012). WHO Classification of Tumours of the Breast, Fourth Edition (Lyon: International Agency for Research on Cancer).

Lanzerath, D. (2011). EUREC - Information - Germany. http://www.eurecnet.org/information/germany.htm.

Lanzerath, D. (2016). EUREC - background. http://www.eurecnet.org/background.

Lee, G.Y., Kenny, P.A., Lee, E.H., and Bissell, M.J. (2007). Three-dimensional culture models of normal and malignant breast epithelial cells. Nat. Methods *4*, 359–365.

Lee, J.M., Ledermann, J.A., and Kohn, E.C. (2014). PARP Inhibitors for BRCA1/2 mutation-associated and BRCA-like malignancies. Ann. Oncol. *25*, 32–40.

Leek, J.T., Johnson, W.E., Parker, H.S., Fertig, E.J., Jaffe, A.E., Storey, J.D., Zhang, Y., and Torres, L.C. (2017). sva: surrogate variable analysis. R package version 3.26.0.

Li, H., and Durbin, R. (2009). Fast and accurate short read alignment with Burrows-Wheeler transform. Bioinformatics *25*, 1754–1760.

Liu, X., Ory, V., Chapman, S., Yuan, H., Albanese, C., Kallakury, B., Timofeeva, O.A., Nealon, C., Dakic, A., Simic, V., et al. (2012). ROCK inhibitor and feeder cells induce the conditional reprogramming of epithelial cells. Am. J. Pathol. *180*, 599–607.

Lorsch, J.R., Collins, F.S., and Lippincott-Schwartz, J. (2014). Cell biology. Fixing problems with cell lines. Science *346*, 1452–1453.

Love, M.I., Huber, W., and Anders, S. (2014). Moderated estimation of fold change and dispersion for RNA-seq data with DESeq2. Genome Biol. *15*, 550.

Martincorena, I., and Campbell, P.J. (2015). Somatic mutation in cancer and normal cells. Science *349*, 1483–1489.

McKenna, A., Hanna, M., Banks, E., Sivachenko, A., Cibulskis, K., Kernytsky, A., Garimella, K., Altshuler, D., Gabriel, S., Daly, M., and DePristo, M.A. (2010). The Genome Analysis Toolkit: a MapReduce framework for analyzing next-generation DNA sequencing data. Genome Res. *20*, 1297–1303.

Mi, H., Muruganujan, A., Casagrande, J.T., and Thomas, P.D. (2013). Large-scale gene function analysis with the PANTHER classification system. Nat. Protoc. *8*, 1551–1566.

Neal, J.T., and Kuo, C.J. (2016). Organoids as models for neoplastic transformation. Annu. Rev. Pathol. *11*, 199–220.

Nik-Zainal, S., Alexandrov, L.B., Wedge, D.C., Van Loo, P., Greenman, C.D., Raine, K., Jones, D., Hinton, J., Marshall, J., Stebbings, L.A., et al.; Breast Cancer Working Group of the International Cancer Genome Consortium (2012). Mutational processes molding the genomes of 21 breast cancers. Cell *149*, 979–993.

Nik-Zainal, S., Davies, H., Staaf, J., Ramakrishna, M., Glodzik, D., Zou, X., Martincorena, I., Alexandrov, L.B., Martin, S., Wedge, D.C., et al. (2016). Landscape of somatic mutations in 560 breast cancer whole-genome sequences. Nature *534*, 47–54.

Ootani, A., Li, X., Sangiorgi, E., Ho, Q.T., Ueno, H., Toda, S., Sugihara, H., Fujimoto, K., Weissman, I.L., Capecchi, M.R., and Kuo, C.J. (2009). Sustained in vitro intestinal epithelial culture within a Wnt-dependent stem cell niche. Nat. Med. *15*, 701–706.

Parker, J.S., Mullins, M., Cheang, M.C., Leung, S., Voduc, D., Vickery, T., Davies, S., Fauron, C., He, X., Hu, Z., et al. (2009). Supervised risk predictor of breast cancer based on intrinsic subtypes. J. Clin. Oncol. *27*, 1160–1167.

Pereira, B., Chin, S.F., Rueda, O.M., Vollan, H.K., Provenzano, E., Bardwell, H.A., Pugh, M., Jones, L., Russell, R., Sammut, S.J., et al. (2016). The somatic mutation profiles of 2,433 breast cancers refines their genomic and transcriptomic landscapes. Nat. Commun. *7*, 11479.

Roskoski, R., Jr. (2014). The ErbB/HER family of protein-tyrosine kinases and cancer. Pharmacol. Res. *79*, 34–74.

Sachs, N., and Clevers, H. (2014). Organoid cultures for the analysis of cancer phenotypes. Curr. Opin. Genet. Dev. *24*, 68–73.

Sato, T., and Clevers, H. (2015). SnapShot: growing organoids from stem cells. Cell *161*, 1700–1700.e1.

Sato, T., Vries, R.G., Snippert, H.J., van de Wetering, M., Barker, N., Stange, D.E., van Es, J.H., Abo, A., Kujala, P., Peters, P.J., and Clevers, H. (2009). Single Lgr5 stem cells build crypt-villus structures in vitro without a mesenchymal niche. Nature *459*, 262–265.

Sato, T., Stange, D.E., Ferrante, M., Vries, R.G., Van Es, J.H., Van den Brink, S., Van Houdt, W.J., Pronk, A., Van Gorp, J., Siersema, P.D., and Clevers, H. (2011). Long-term expansion of epithelial organoids from human colon, adenoma, adenocarcinoma, and Barrett's epithelium. Gastroenterology *141*, 1762–1772.

Saunders, C.T., Wong, W.S., Swamy, S., Becq, J., Murray, L.J., and Cheetham, R.K. (2012). Strelka: accurate somatic small-variant calling from sequenced tumor-normal sample pairs. Bioinformatics *28*, 1811–1817.

Schmidt, M., Thomssen, C., and Untch, M. (2016). Intrinsic subtypes of primary breast cancer–gene expression analysis. Oncol. Res. Treat. *39*, 102–110.

Sharma, S.V., Haber, D.A., and Settleman, J. (2010). Cell line-based platforms to evaluate the therapeutic efficacy of candidate anticancer agents. Nat. Rev. Cancer *10*, 241–253.

Shaw, K.R., Wrobel, C.N., and Brugge, J.S. (2004). Use of three-dimensional basement membrane cultures to model oncogene-induced changes in mammary epithelial morphogenesis. J. Mammary Gland Biol. Neoplasia *9*, 297–310.

Sherry, S.T., Ward, M.H., Kholodov, M., Baker, J., Phan, L., Smigielski, E.M., and Sirotkin, K. (2001). dbSNP: the NCBI database of genetic variation. Nucleic Acids Res. *29*, 308–311.

Soysal, S.D., Tzankov, A., and Muenst, S.E. (2015). Role of the tumor microenvironment in breast cancer. Pathobiology *82*, 142–152.

Spitzer, M., Wildenhain, J., Rappsilber, J., and Tyers, M. (2014). BoxPlotR: a web tool for generation of box plots. Nat. Methods *11*, 121–122.

Stein, C.K., Qu, P., Epstein, J., Buros, A., Rosenthal, A., Crowley, J., Morgan, G., and Barlogie, B. (2015). Removing batch effects from purified plasma cell gene expression microarrays with modified ComBat. BMC Bioinformatics *16*, 63.

Stewart, B.W., and Wild, C. (2014). World Cancer Report 2014 (World Health Organization).

Troyer, K.L., and Lee, D.C. (2001). Regulation of mouse mammary gland development and tumorigenesis by the ERBB signaling network. J. Mammary Gland Biol. Neoplasia *6*, 7–21.

van de Wetering, M., Francies, H.E., Francis, J.M., Bounova, G., Iorio, F., Pronk, A., van Houdt, W., van Gorp, J., Taylor-Weiner, A., Kester, L., et al. (2015). Prospective derivation of a living organoid biobank of colorectal cancer patients. Cell *161*, 933–945.

Van der Auwera, G.A., Carneiro, M.O., Hartl, C., Poplin, R., Del Angel, G., Levy-Moonshine, A., Jordan, T., Shakir, K., Roazen, D., Thibault, J., et al. (2013). From FastQ data to high confidence variant calls: the Genome Analysis Toolkit best practices pipeline. Curr. Protoc. Bioinformatics *43*, 11.10.11-33.

Vargo-Gogola, T., and Rosen, J.M. (2007). Modelling breast cancer: one size does not fit all. Nat. Rev. Cancer *7*, 659–672.

Verissimo, C.S., Overmeer, R.M., Ponsioen, B., Drost, J., Mertens, S., Verlaan-Klink, I., Gerwen, B.V., van der Ven, M., Wetering, M.V., Egan, D.A., et al. (2016). Targeting mutant RAS in patient-derived colorectal cancer organoids by combinatorial drug screening. eLife *5*, e18489.

Wansbury, O., Panchal, H., James, M., Parry, S., Ashworth, A., and Howard, B. (2008). Dynamic expression of Erbb pathway members during early mammary gland morphogenesis. J. Invest. Dermatol. *128*, 1009–1021.

Whittle, J.R., Lewis, M.T., Lindeman, G.J., and Visvader, J.E. (2015). Patient-derived xenograft models of breast cancer and their predictive power. Breast Cancer Res. *17*, 17.

Yang, Y., Spitzer, E., Meyer, D., Sachs, M., Niemann, C., Hartmann, G., Weidner, K.M., Birchmeier, C., and Birchmeier, W. (1995). Sequential requirement of hepatocyte growth factor and neuregulin in the morphogenesis and differentiation of the mammary gland. J. Cell Biol. *131*, 215–226.

Zack, T.I., Schumacher, S.E., Carter, S.L., Cherniack, A.D., Saksena, G., Tabak, B., Lawrence, M.S., Zhsng, C.Z., Wala, J., Mermel, C.H., et al. (2013). Pan-cancer patterns of somatic copy number alteration. Nat. Genet. *45*, 1134–1140.

Zardavas, D., Baselga, J., and Piccart, M. (2013). Emerging targeted agents in metastatic breast cancer. Nat. Rev. Clin. Oncol. *10*, 191–210.

## STAR★METHODS

### KEY RESOURCE TABLE

| REAGENT or RESOURCE | SOURCE | IDENTIFIER |
|---|---|---|
| Antibodies | | |
| Anti-Estrogen Receptor alpha antibody [SP1] | Abcam | Cat# ab27595 |
| Progesterone Receptor antibody | DAKO | Cat# M3569 |
| HER-2/c-erB-2/neu, Rabbit Monoclonal Antibody | Thermo Scientific | Cat# RM-9103-S1 |
| Biological Samples | | |
| Human breast cancer tissue | This study | Table S1 |
| Human blood samples | This study | Table S1 |
| Chemicals, Peptides, and Recombinant Proteins | | |
| Afatinib (BIBW2992) | Selleckchem | Cat# S1011 |
| Gefitinib (ZD1839) | Selleckchem | Cat# S1025 |
| Pictilisib (GDC-0941) | Selleckchem | Cat# S1065 |
| Ipatasertib (GDC-0068) | Selleckchem | Cat# S2808 |
| AZD8055 | Selleckchem | Cat# S1555 |
| Everolimus (RAD001) | Selleckchem | Cat# S1120 |
| Olaparib (AZD2281, Ku-0059436) | Selleckchem | Cat# S1060 |
| Niraparib (MK-4827) | Selleckchem | Cat# S2741 |
| Tamoxifen | Sigma | Cat# T5648 |
| Nutlin-3 | Cayman Chemical | Cat# 10004372 |
| Colcemid | GIBCO | Cat# 152120-12 |
| R-Spondin 1 | Peprotech | Cat# 120-38 |
| Neuregulin 1 | Peprotech | Cat# 100-03 |
| FGF 7 | Peprotech | Cat# 100-19 |
| FGF 10 | Peprotech | Cat# 100-26 |
| EGF | Peprotech | Cat# AF-100-15 |
| Noggin | Peprotech | Cat# 120-10C |
| A83-01 | Tocris | Cat# 2939 |
| Y-27632 | Abmole | Cat# Y-27632 |
| SB202190 | Sigma | Cat# S7067 |
| B27 supplement | GIBCO | Cat# 17504-44 |
| N-Acetylcysteine | Sigma | Cat# A9165-5g |
| Nicotinamide | Sigma | Cat# N0636 |
| Critical Commercial Assays | | |
| MycoAlert mycoplasma detection kit | Lonza | Cat# LT07-318 |
| DNeasy blood & tissue kit | QIAGEN | Cat# 69506 |
| RNeasy mini kit | QIAGEN | Cat# 74104 |
| Truseq Stranded Total RNA kit with Ribo-Zero Human/Mouse/Rat set A and B | Illumina | Cat# RS-122-2201 and Cat# RS-122-2202 |
| Qubit dsDNA HS Assay Kit | Thermo Fisher | Cat# Q32854 |
| CellTiter-Glo 3D Cell Viability Assay | Promega | Cat# G9681 |
| Deposited Data | | |
| Human gene definitions for GRCh37 | Ensembl | http://ftp.ensemblorg.ebi.ac.uk/pub/release-74/gtf/homo_sapiens/Homo_sapiens.GRCh37.74.gtf.gz |
| BAM files for DNA and RNA sequencing data | This study, EGA | https://www.ebi.ac.uk/ega/studies/EGAS00001002158 |

(*Continued on next page*)

*Continued*

| REAGENT or RESOURCE | SOURCE | IDENTIFIER |
|---|---|---|
| Human reference genome NCBI build 37, GRCh37 | Genome Reference Consortium | https://www.ncbi.nlm.nih.gov/projects/genome/assembly/grc/human/ |
| Level 3 RNA-seq BC data | TCGA Data Portal | N/A |
| Signatures of Mutational Processes in Human Cancer | COSMIC | http://cancer.sanger.ac.uk/cosmic/signatures |
| Experimental Models: Cell Lines | | |
| Breast cancer organoid lines | This study, http://hub4organoids.eu | Tables S1, S2, and S3 |
| Experimental Models: Organisms/Strains | | |
| NMRI Nude Mouse Crl:NMRI-Foxn1nu | Charles Rivers | http://www.criver.com/products-services/basic-research/find-a-model/nmri-nude |
| Oligonucleotides | | |
| TP53 gRNA | Drost et al., 2015 | GACGGAAACCGTAGCTGCC |
| TP53_for | Drost et al., 2015 | CAGGAAGCCAAAGGGTGAAGA |
| TP53_rev | Drost et al., 2015 | CCCATCTACAGTCCCCCTTG |
| Recombinant DNA | | |
| pSpCas9(BB)-2A-GFP | Addgene | plasmid # 48138 |
| pGEM-T Easy vector system I | Promega | Cat# A1360 |
| Software and Algorithms | | |
| BoxPlotR | Spitzer et al., 2014 | N/A |
| Illumina analysis pipeline v 1.2.1 | Cuppen lab | https://github.com/UMCUGenetics/IAP |
| Genome Analysis Toolkit (GATK) v3.2.2 | McKenna et al., 2010 | https://github.com/broadinstitute/gatk |
| Burrows-Wheeler Alignment with maximal exact matches (BWA-MEM) v0.7.5a | Li and Durbin, 2009 | http://bio-bwa.sourceforge.net/ |
| Strelka (v1.0.14) | Saunders et al., 2012 | ftp://ftp.illumina.com/v1-branch/v1.0.14/ |
| VarScan (v2.4.1) | Koboldt et al., 2012 | http://varscan.sourceforge.net/ |
| FreeBayes (v1.0.2) | Garrison and Marth, 2012 | https://github.com/ekg/freebayes |
| MuTect (v1.1.7) | Cibulskis et al., 2013 | https://github.com/broadinstitute/mutect |
| MutationalPatterns R package, release 3.4 | Blokzijl et al., 2016a | https://github.com/UMCUGenetics/MutationalPatterns |
| SnpEff (v4.1) | Cingolani et al., 2012 | http://snpeff.sourceforge.net/ |
| dbSNP (v137) | Sherry et al., 2001 | ftp://ftp.ncbi.nih.gov/snp/ |
| Control-FREEC v7.2 | Boeva et al., 2012 | https://github.com/BoevaLab/FREEC |
| RNA analysis pipeline v2.1.0 | Cuppen lab | https://github.com/UMCUGenetics/RNASeq |
| FastQC (v0.11.4) | Babraham bioinformatics | https://www.bioinformatics.babraham.ac.uk/projects/fastqc/fastqc_v0.11.4_source.zip |
| STAR (v2.4.2a) | Dobin et al., 2013 | https://github.com/alexdobin/STAR |
| Picard (v1.141) | Broad Institute | https://github.com/broadinstitute/picard |
| HTSeq-count (v0.6.1) | Anders et al., 2015 | https://github.com/simon-anders/htseq |
| DESeq2 R package | Love et al., 2014 | http://bioconductor.org/packages/release/bioc/html/DESeq2.html |
| ComBat | Leek et al., 2017 | http://bioconductor.org/packages/release/bioc/html/sva.html |
| PAM50 | Parker et al., 2009 | N/A |
| SCMGENE | Haibe-Kains et al., 2012 | N/A |
| SCMOD1 | Desmedt et al., 2008 | N/A |
| IntClust | Ali et al., 2014 | https://cran.r-project.org/web/packages/IntClust/index.html |

(*Continued on next page*)

*Continued*

| REAGENT or RESOURCE | SOURCE | IDENTIFIER |
|---|---|---|
| genefu R package | Gendoo et al., 2016 | https://www.bioconductor.org/packages/release/bioc/html/genefu.html |
| CorelDraw X7 | Corel Corporation | N/A |
| Other | | |
| Cultrex growth factor reduced BME type 2 | Trevigen | Cat# 3533-010-02 |
| Collagenase | Sigma | Cat# C9407 |

## CONTACT FOR REAGENT AND RESOURCE SHARING

Further information and requests for resources and reagents should be directed to and will be fulfilled by the Lead Contact, Hans Clevers (h.clevers@hubrecht.eu). Biobanked organoids will be cataloged at the HUB foundation for Organoid Technology http://hub4organoids.eu and can be requested at info@hub4organoids.eu. Distribution of organoids to third (academic or commercial) parties requires completion of a material transfer agreement and will have to be authorised by the medical ethical committee UMCU at request of the HUB in order to ensure compliance with the Dutch medical research involving human subjects' act. Use of organoids is subjected to patient consent; upon consent withdrawal, distributed organoid lines and any derived material will have to be promptly disposed of.

## EXPERIMENTAL MODELS AND SUBJECT DETAILS

### Approval of studies involving humans and patient informed consent

The collection of BC patient data and tissue for the generation and distribution of BC organoids has been performed according to the guidelines of the European Network of Research Ethics Committees (EUREC) following European, national, and local law (Lanzerath, 2016). In the Netherlands, the responsible accredited ethical committees reviewed and approved the studies in accordance with the '*Wet medisch-wetenschappelijk onderzoek met mensen'* (medical research involving human subjects act) (Borst-Eilers and Sorgdrager, 1998). The medical ethical committee UMC Utrecht (METC UMCU) approved protocol 12-427/C for the establishment of mammary gland organoid cultures as well as biobanking protocol HUB-Cancer TcBio#12-093. In Germany, the legal competence of the research ethical committees is restricted to drug research and to research on medicinal devices (Lanzerath, 2011). Patients were exclusively recruited in the federal state of Hamburg, Germany where approval of anonymised biomedical research by an ethical committee is not required (Ethik Kommission Ärztekammer Hamburg, 2015). All patients participating in the biobank study signed informed consent forms approved by the responsible authority (see above). In all cases, patients can withdraw their consent at any time, leading to the prompt disposal of their tissue and any derived material. Patients participating under protocol 12-427/C did not sign informed consent since derived organoids were not biobanked. Biobanked organoids will be cataloged at http://hub4organoids.eu and can be requested at info@hub4organoids.eu. Distribution of organoids to third (academic or commercial) parties will have to be authorised by the METC UMCU at request of the HUB in order to ensure compliance with the Dutch medical research involving human subjects' act. Clinical information is available in Table S1. Age, weight, and height of subjects can be inquired through info@hub4organoids.eu.

### BC tissue processing

Upon arrival, BC tissues were photographed and cut into 1-3 $mm^3$ pieces. Two random pieces were snap frozen and stored at −80°C for DNA isolation, two random pieces were fixed in formalin for histopathological analysis and immunohistochemistry, and the remainder was processed for the isolation of viable cells. The remaining tissue was minced, washed with 10 mL AdDF+++ (Advanced DMEM/F12 containing 1x Glutamax, 10 mM HEPES, and antibiotics) and digested in 10 mL BC organoid medium (Table S2) containing 1-2 $mg \cdot ml^{-1}$ collagenase (Sigma, C9407) on an orbital shaker at 37°C for 1-2 h. The digested tissue suspension was sequentially sheared using 10 mL and 5 mL plastic and flamed glass Pasteur pipettes. After every shearing step the suspension was strained over a 100 μm filter with retained tissue pieces entering a subsequent shearing step with ~10ml AdDF+++. 2% FCS were added to the strained suspension before centrifugation at 400 *rcf.* The pellet was resuspended in 10ml AdDF+++ and centrifuged again at 400 *rcf.* In case of a visible red pellet, erythrocytes were lysed in 2 mL red blood cell lysis buffer (Roche, 11814389001) for 5 min at room temperature before the addition of 10ml AdDF+++ and centrifugation at 400 *rcf.* Needle biopsies of metastatic BC lesions were processed as above following removal of macroscopically obvious non tumor tissue (e.g., liver).

### BC organoid culture

The pellet was resuspended in 10 $mg \cdot ml^{-1}$ cold Cultrex growth factor reduced BME type 2 (Trevigen, 3533-010-02) and 40 μL drops of BME-cell suspension were allowed to solidify on prewarmed 24-well suspension culture plates (Greiner, M9312) at 37°C for 20 min.

Upon completed gelation, 400 μL of BC organoid medium (Table S2) was added to each well and plates transferred to humidified 37°C / 5% $CO_2$ incubators at either 2% or ambient $O_2$. Medium was changed every 4 days and organoids were passaged every 1-4 weeks: cystic organoids were resuspended in 2 mL cold AdDF+++ and mechanically sheared through flamed glass Pasteur pipettes. Dense organoids were dissociated by resuspension in 2 mL TrypLE Express (Invitrogen, 12605036), incubation for 1-5 min at room temperature, and mechanical shearing through flamed glass Pasteur pipettes. Following the addition of 10 mL AdDF+++ and centrifugation at 300 *rcf.* or 400 *rcf.* respectively, organoid fragments were resuspended in cold BME and reseeded as above at ratios (1:1 to 1:6) allowing the formation of new organoids. Single cell suspensions were initially seeded at high density and reseeded at a lower density after ~1 week. In order to prevent misidentification and/or cross-contamination of BC organoids, we cultured every line physically separate, implemented the use of a laboratory management system, and validated the identity of biobanked organoid lines by single-nucleotide polymorphism (SNP) based fingerprinting. All organoid lines tested negative in the MycoAlert mycoplasma detection kit (Lonza, LT07-318).

### Xeno-transplantations

Organoids were split, strained < 70 μm, and allowed to grow for 5-7 days. Organoids were harvested and injected into the fourth mammary fat pads of NMRI-Nude mice (Charles Rivers) at $10^6$ cells in 40 μL of complete BC organoid medium/BME (1:1). Mice with established tumors (average volume of approx. 50 $mm^3$) were treated with vehicle or afatinib (12.5 $mg \cdot kg^{-1}$, orally, 5 days on, 2 days off) for 4 weeks. Animals were sacrificed with $CO_2$ before combined tumors reached a volume of 1,500 $mm^3$. For *in vivo* dosing, afatinib was dissolved in 1.8% hydroxypropyl-b-cyclodextrin (Sigma), 5% of a 10% acetic acid stock, and 0.5% aqueous natrosol. Mammary tumor size was determined 3 times a week by caliper measurements (length and width in mm), and tumor volume (in $mm^3$) was calculated by using the following formula: $0.5 \cdot length \cdot width^2$. Data is expressed as the 7 day moving average of these measurements. This study was approved by the Animal Ethics Committee of the Netherlands Cancer Institute (DEC-NKI; OZP = 12012, WP5720), complying with Dutch legislation.

## METHOD DETAILS

### Histology and imaging

Tissue and organoids were fixed in 4% paraformaldehyde followed by dehydration, paraffin embedding, sectioning, and standard HE staining. Sections were randomized and blindly analyzed by a breast cancer pathologist. Immunohistochemistry was performed using antibodies against ERα (Abcam, ab27595, 1:5), PR (DAKO, M3569, 1:150), and HER2 (Thermo, RM-9103-S1, 1:100). Images were acquired on a Leica Eclipse E600 microscope and processed using the Adobe Creative Cloud software package. Time lapse bright-field imaging was performed on a Leica AF7000 fluorescence microscope equipped with a Leica DFC420C camera at 37°C and 5% humidified $CO_2$.

### Genomic analysis

For karyotyping, 0.1 $\mu g \cdot ml^{-1}$ colcemid (GIBCO, 152120-12) was added to the medium of expanding organoids. The following day organoids were harvested, trypsinized to single cells, incubated in hypotonic 75 mM KCl solution, and fixed in methanol: acetic acid in (3:1). Metaphase spreads were prepared, stained with 5 $\mu g \cdot ml^{-1}$ DAPI (Sigma, D9542), imaged on a Leica SP8 confocal microscope, and quantified by manual chromosome counting. Data was visualized using BoxPlotR (Spitzer et al., 2014) and CorelDraw X7. gDNA was isolated from primary tissue, blood/PBMCs, and organoids using the DNeasy blood & tissue kit (QIAGEN) with 1 μg per sample being used to generate DNA libraries for Illumina WGS using standard protocols (Illumina). No sample size estimate was calculated. The libraries were sequenced with paired-end (2 × 100 bp) runs using Illumina HiSeq X Ten sequencers to 30X to an average of 39.9X (SD 4.5). Illumina data was processed with our in-house developed pipeline v 2.2.1 (https://github.com/UMCUGenetics/IAP/releases/tag/v2.2.1) including somatic mutation analysis (Strelka, VarScan, FreeBayes, and MuTect) and the Genome Analysis Toolkit (GATK) v3.2.2 (McKenna et al., 2010) according to best practices guidelines (Van der Auwera et al., 2013). Sequence reads were mapped against human reference genome GRCh37 using Burrows-Wheeler Alignment with maximal exact matches (BWA-MEM) v0.7.5a (Li and Durbin, 2009) followed by marked duplicates, merging of lanes, and realignment of indels. Base recalibration was not performed. Somatic mutations were determined by providing the reference and tumor or organoid sequencing data to the following algorithms: Strelka (v1.0.14) (Saunders et al., 2012), VarScan (v2.4.1) (Koboldt et al., 2012), FreeBayes (v1.0.2) (Garrison and Marth, 2012), and MuTect (v1.1.7) (Cibulskis et al., 2013). See CPCT.ini file (https://github.com/UMCUGenetics/IAP/blob/v2.2.1/settings/CPCT.ini) for full details. High-confident variants were determined by the tools' default filtering steps and merged to a single *vcf.* file. Mutational signatures were analyzed similar to Blokzijl et al. (2016a): genomic context was determined for all high quality somatic SNVs (read depth > = 20, called by at least 2 independent callers) using the MutationalPatterns R package, release 3.4 (Blokzijl et al., 2016b). This package was also used to determine the contribution of "signatures of mutational processes in human cancer" (source http://cancer.sanger.ac.uk/cosmic/signatures) in BC tissue and organoid samples. Effect predictions and annotations were added using SnpEff(v4.1) (Cingolani et al., 2012) and dbSNP (v137) (Sherry et al., 2001). To detect CNAs, BAM files were analyzed for read-depth variations by Control-FREEC v7.2 (Boeva et al., 2012) with a bin size of 1kb. Highly variable regions (CNVs in at least 3 control samples) were excluded from the analysis, as were CNVs present in respective reference samples. To obtain high quality somatic CNAs highly variable regions (CNAs in at least 3 control samples) were

excluded from the analysis, as were CNAs present in respective reference samples. Gene bodies were defined using CDS definitions of cancer genes identified as $p < 0.05$ by Zack et al. (2013). The average gene ratio per frequently mutated gene body was calculated and divided by the average ratio in control samples to normalize and adjust for gene specific biases in copy numbers. Per sample and frequently mutated cancer gene, the most deleterious variant was identified based on SnpEff (v4.1) effect prediction (Cingolani et al., 2012), details in online code https://github.com/UMCUGenetics/SmallTools/blob/master/Make_Somatic_Mutation_Overview.py. Gene bodies were defined using CDS definitions of cancer genes identified as significantly mutated in Cancer Genome Atlas (2012), mutated at a frequency $\geq$ 5% in Pereira et al. (2016), and/or being among the top 10 mutated genes in Nik-Zainal et al. (2016). Accession number: EGA: EGAS00001002158.

## RNA-seq analysis

Total RNA was isolated from organoids 4-6 days after passaging using the RNeasy mini kit (QIAGEN). Quality and quantity of isolated RNA was checked and measured with Bioanalyzer2100 RNA Nano 6000 chips (Agilent, Cat. 5067-1511). Library preparation was started with 500ng of Total RNA using the Truseq Stranded Total RNA kit with Ribo-Zero Human/Mouse/Rat set A and B by Illumina (Cat. RS-122-2201 and RS-122-2202). After the library preparation libraries were checked with Bioanalyzer2100 DNA High Sensitivity chips (Cat. 5067-4626) and with Qubit (Qubit dsDNA HS Assay Kit, Cat. Q32854). Libraries were equimolar pooled to 2 nM. And sequenced on the Illumina Nextseq, 2x75bp high output, and 1.0-1.4 pM of library pools was loaded. Samples were sequenced to average depth of 22.2 million fragments (SD 7.2 million). After sequencing quality control, mapping and counting analyses were performed using our in-house RNA analysis pipeline v2.1.0 (https://github.com/UMCUGenetics/RNASeq), based on best practices guidelines (https://software.broadinstitute.org/gatk/documentation/article.php?id=3891). In short, sequence reads were checked for quality by FastQC (v0.11.4) after which reads were aligned to GRCh37 using STAR (v2.4.2a) and add read groups using Picard perform quality control on generated BAM files using Picard (v1.141). Samples passing QC were then processed to count reads in features using HTSeq-count (v0.6.1) (Anders et al., 2015). After read counting genes (ENSEMBL definitions GRCh37, release 74) with zero raw read counts for all samples were removed (23375 genes out of 63677), resulting in a 40302 genes by 22 samples counts matrix with Ensembl gene identifiers. The median-of-ratios method from the DESeq2 R package (Love et al., 2014) was used to normalize all samples for sequencing depth. We first mapped the Ensembl identifiers to gene symbols using the biomaRt R package (Durinck et al., 2009). After removing genes with no corresponding gene symbols and duplicate mappings, we obtained a counts matrix of 25991 genes by 22 samples with gene symbol identifiers. We downloaded Level 3 RNA-seq BC data from the TCGA Data Portal on June 25$^{th}$, 2015 and matched clinical data on November 12$^{th}$, 2015. This included 1102 samples, annotated with age, histology, TNM stage, ER, PR, and HER2 status. The TCGA count data was used for analysis as provided, namely with RNA-seq by expectation maximization normalized counts. We normalized expression data of organoids and TCGA tumors together using a modified version of ComBat (Johnson et al., 2007; Stein et al., 2015). We chose the TCGA expression dataset as reference and normalized organoid expression accordingly. Following normalization for sequencing depth and $\log_2$-transformation, organoids and TCGA samples were subtyped independently using four algorithms: PAM50 (Parker et al., 2009), SCMGENE (Haibe-Kains et al., 2012), SCMOD1 (Desmedt et al., 2008), and IntClust (Ali et al., 2014). Subtypes were color-coded and shown as annotation rows in Figure 5B. We used implementations of the four algorithms in the genefu R package (Gendoo et al., 2016). All classifiers were used with their default robust scaling option. Differential expression comparison using the DESeq2 R package (Love et al., 2014) was performed of discohesive organoid lines 13T, 36T, 66T, 74T, and 95T versus all other organoids with available gene expression data. Statistical overrepresentation was quantified with the PANTHER classification system (Mi et al., 2013).

## Gene editing

Organoids derived from preventive mastectomy (144-PM) were dissociated into small clumps using pre-warmed Accutase (STEMCELL Technologies #07920), washed once with Advanced DMEM/F12 +++ and twice with Opti-MEM. Cells were suspended with 100μl Opti-MEM containing RHO/ROCK pathway inhibitor (10 μM) and 10 μg of pSpCas9(BB)-2A-GFP (Addgene plasmid # 48138) with gRNA targeting *TP53* (GACGGAAACCGTAGCTGCC) (Drost et al., 2015) and transferred into 2mm gap NEPA electroporation cuvette (Lot No. 2S1509). For electroporation, we utilized NEPA21 type-II electroporator with the following setup:

| Poring Pulse | | | | | | Transfer Pulse | | | | | |
|---|---|---|---|---|---|---|---|---|---|---|---|
| V | Length (ms) | Interval (ms) | No. | D. Rate (%) | Polarity | V | Length (ms) | Interval (ms) | No. | D. Rate (%) | Polarity |
| 175 | 7.5 | 50 | 2 | 10 | + | 20 | 50 | 50 | 5 | 40 | +/− |

Following electroporation, 300μl of complete growth medium was added to the cells and they were incubated in room temperature for 15 minutes. Cells were centrifuged, suspended in 200μl BME and plated as previously described. Complete medium was added after cell-BME suspension drops had solidified. 2-3 days after electroporation 10 μM Nutlin-3 (Cayman Chemical) was added to the growth medium. 2-3 weeks after electroporation, single organoids were picked and transferred into 1.5ml microcentrifuge tubes containing 200 μL of pre-warmed Accutase. Following 2-3 minutes incubation, organoids were sheared into small cell clumps by

pipetting, washed with 1ml Advanced DMEM/F-12 +++ and centrifuged for 5 minutes in 2000rpm. Cells were resuspended with 40 μL BME and plated. For genotyping, genomic DNA was isolated using Viagen Direct PCR (Viagen). GoTaq Flexi DNA polymerase (Promega) was used for PCR amplification. Primer sequences: P53_for, 5′-CAGGAAGCCAAAGGGTGAAGA-3′ P53_rev, 5′-CCCATCTA CAGTCCCCCTTG-3′. Products were cloned into pGEM-T Easy vector system I (Promega) and sequenced using T7 sequencing primer. Three clonal *TP53* mutant lines were generated. See also Figure S4.

### Drug screen

Organoids were split, strained < 70 μm, and allowed to grow for 5-7 days. Organoids were harvested and diluted to 75 organoids/μl in growth medium containing 5% BME. Using a Multidrop combi reagent dispenser (ThermoFisher) black, clear bottom 384-well plates (Corning) were coated with 10 μL BME before the addition of 30 μL organoid suspension. Then, 21 concentrations of afatinib, gefitinib, pictilisib, GDC-0068, AZD8055, everolimus (all Selleckchem), or tamoxifen (Sigma) as well as DMSO controls were added in duplicate using a Tecan D300e digital dispenser (Life Sciences). To measure ATP as proxy for viable cells, 40 μL of CellTiter-Glo 3D Reagent (Promega) per well were added after five days, before shaking the plate for 30 min at room temperature and reading luminescence on a SpectraMax microplate reader (Molecular Devices). Data was analyzed using GraphPad Prism 6 followed by manual determination of $IC_{50}$ values (absolute for homogeneous populations, relative for heterogeneous populations). Averages of $IC_{50}$s from two to three independent experiments were calculated and visualized using Morpheus (https://software.broadinstitute.org/morpheus) and CorelDraw X7. For the PARPi assay, organoids were harvested 2-4 days post-seeding, strained < 100 μm, diluted to a concentration of 13-20 organoids/μl in BME and replated in 48 well plates (20 μL of BME per well). Organoids were grown for 2 weeks at the indicated concentrations of olaparib and niraparib in BC medium lacking N-Acetylcysteine and Y-27632. Medium was removed and BME drops were suspended in 100 μL CellTiter-Glo 3D and 80 μL advanced DMEM/F12. Following transfer to 96well black U-shaped plates (Greiner), 5 min shaking and 15 min incubation at RT, luminescence was measured in a plate reader (Centro LB960). Each condition was tested in replicates and results were normalized to the lowest concentration with values ≥ DMSO controls.

## QUANTIFICATION AND STATISTICAL ANALYSIS

Statistical methods are outlined in the respective figure legends were applicable. Statistical analyses were performed with MS Excel and Prism GraphPad. P values were calculated using two-tailed Student's t test assuming a normal sample distribution. Sample size for animal experiments was determined based upon pilot experiments. Investigators were blinded for evaluation of all tissue stainings. Data shown are either representative of two or more independent experiments or combined from two or more independent experiments as indicated. Data is analyzed as mean ± SEM. Sequence analysis details can be found in the respective STAR Methods sections.

## DATA AND SOFTWARE AVAILABILITY

Illumina data processing pipeline v2.2.1 is available under https://github.com/UMCUGenetics/IAP/releases/tag/v2.2.1, RNA analysis pipeline v2.1.0 is available under https://github.com/UMCUGenetics/RNASeq. Details for the detection of somatic mutations can be found under https://github.com/UMCUGenetics/IAP/blob/v2.2.1/settings/CPCT.ini. Deleterious variants were identified using https://github.com/UMCUGenetics/SmallTools/blob/master/Make_Somatic_Mutation_Overview.py. BAM files for DNA and RNA sequencing data are made available through controlled access at the European Genome-phenome Archive (EGA) which is hosted at the EBI and the CRG (https://ega-archive.org), under accession number EGA: EGAS00001002158. Data access requests will be evaluated by the UMCU Department of Genetics Data Access Board (EGAC00001000432) and transferred upon completion of a material transfer agreement and authorization by the medical ethical committee UMCU at request of the HUB in order to ensure compliance with the Dutch 'medical research involving human subjects' act.

Cell

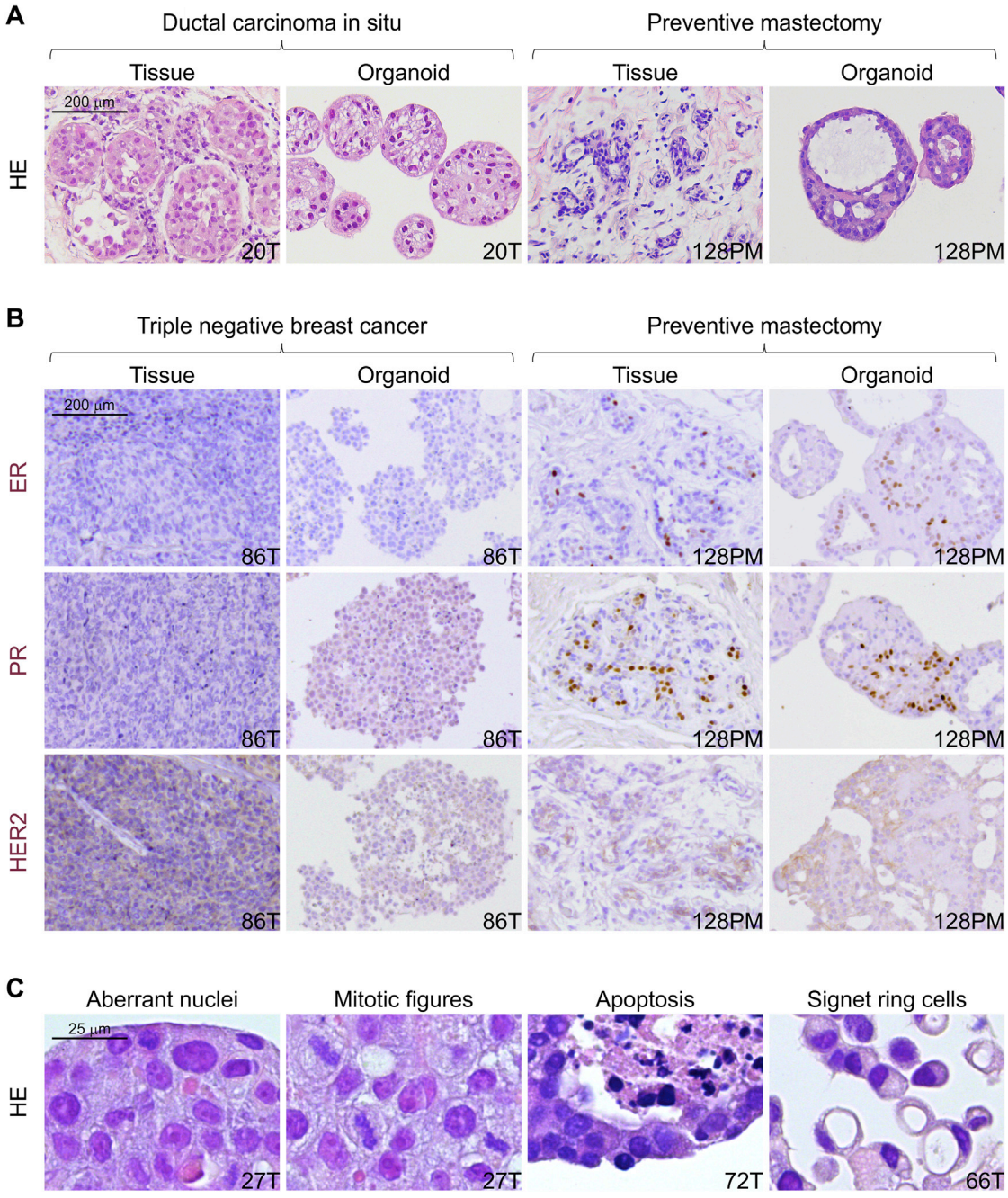


**Figure S1. Additional Histology and Receptor Status, Related to Figure 2**

(A) Comparative histological images of DCIS (left) and PM (right) tissues with their respectively derived organoids lines. DCIS organoids show a cribriform architecture reminiscent of the original lesion, while PM organoids show a mildly hyperplastic, histologically inconspicuous phenotype (Table S3). Scale bar equals 200 µm.

(B) Immunohistochemical receptor status analysis of TNBC (left) and PM (right) tissue-organoid pairs. As expected, the representative TNBC tissue and organoid line present negative for ER, PR, and HER2. The occasional ER and PR positive cells found in PM tissue are retained in the derived organoids, as is HER2 status. Scale bar equals 200 µm.

(C) High power magnifications of BC organoids showing characteristic histological features of tumor cells. From left to right: enlarged and polymorphic nuclei, mitotic figures, apoptosis, and signet ring cells. Scale bar equals 25 µm.

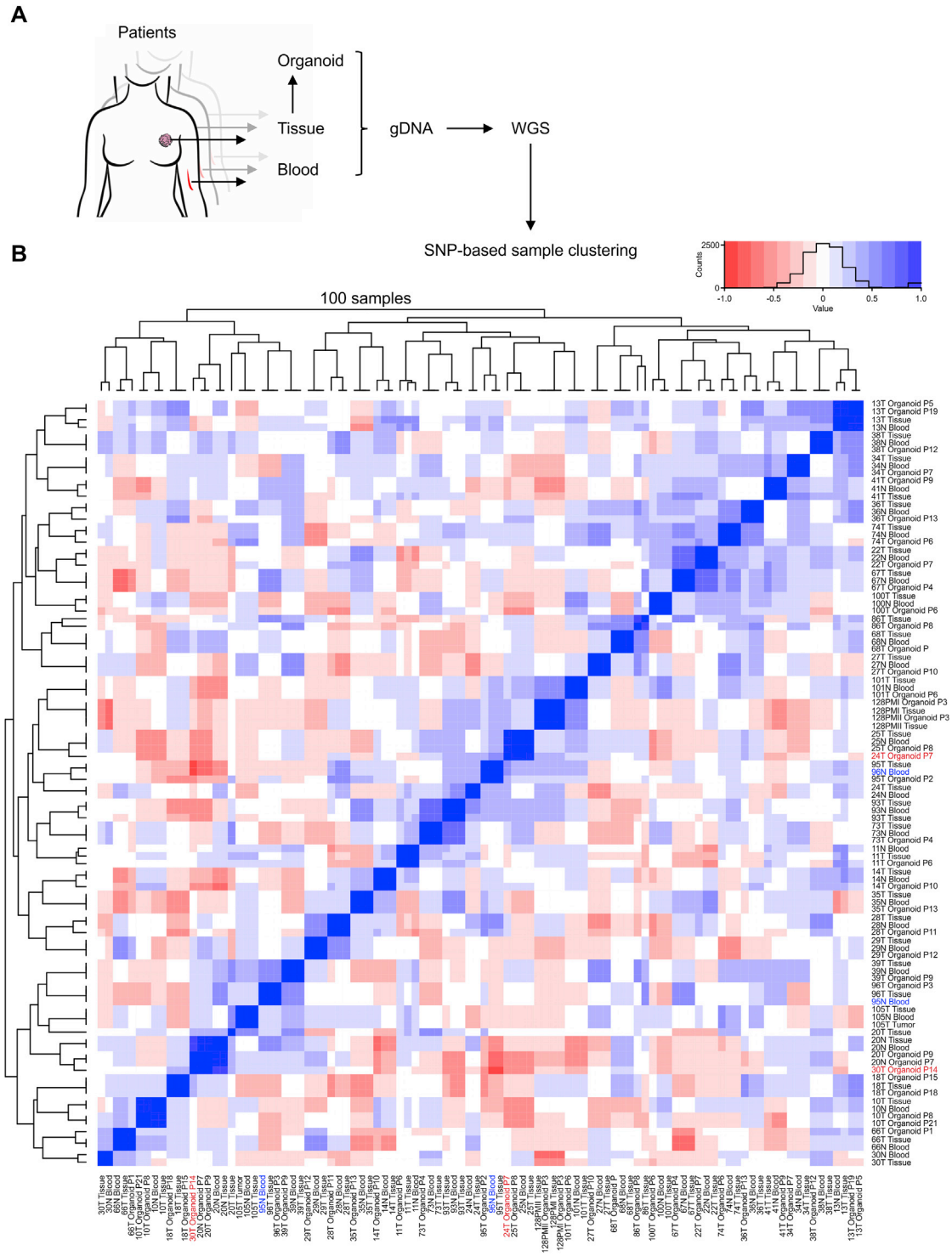


**Figure S2. Genetic Distance of Patient Tissues and Organoids, Related to Figure 3**

(A) Diagram showing the origin of patient specific genomic DNA (gDNA) samples (normal blood, BC tissue, and BC organoids) and their relation to Figure S2B. (B) Hierarchical clustering heat-map visualizing the genetic distance of 100 gDNA samples from 33 patients. Note 29 blocks of three to four correctly clustered samples with matching patient numbers (black font), two swapped blood gDNA samples (blue font), and two cases of cross-contaminated BC organoid lines (red font).

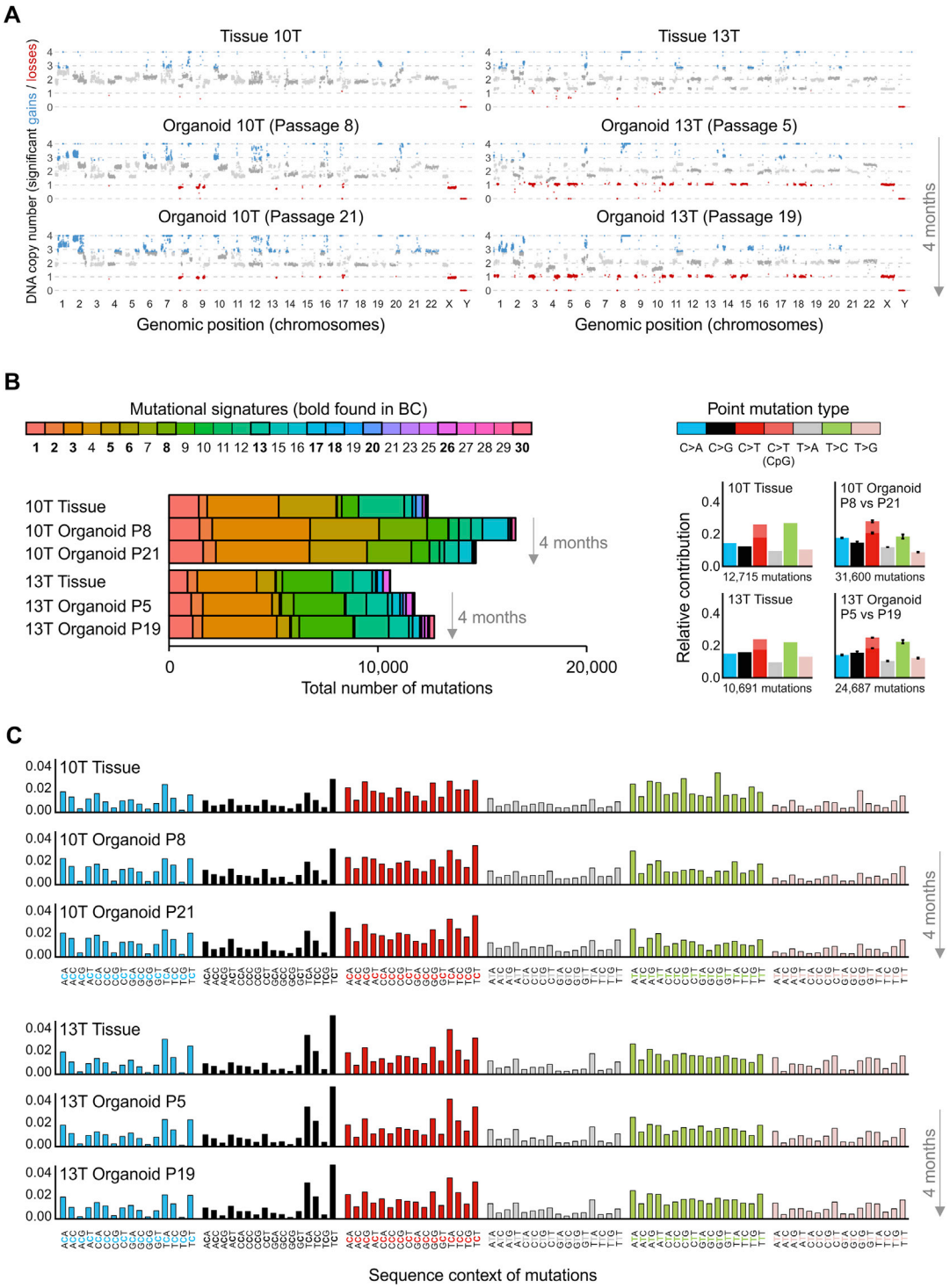


**Figure S3. Additional Genomic Analysis of BC Organoids, Related to Figure 3**

(A) Scatterplots showing genome wide CNAs of BC tissues compared to derived BC organoids at different passages (four months apart, equalling 13 to 14 passages). DNA copy number gains (blue) and losses (red) found in the original BC are conserved in the derived organoid lines irrespective of their passage number. Chromothripsis (multiple rearrangements within single chromosomes) is present in both examples.

(B) Mutational signatures (left) and underlying point mutation types (right) of BC tissues compared to derived BC organoids sampled at the indicated passages four months apart.

(C) Relative contributions of point mutations of the same samples in their sequence context.

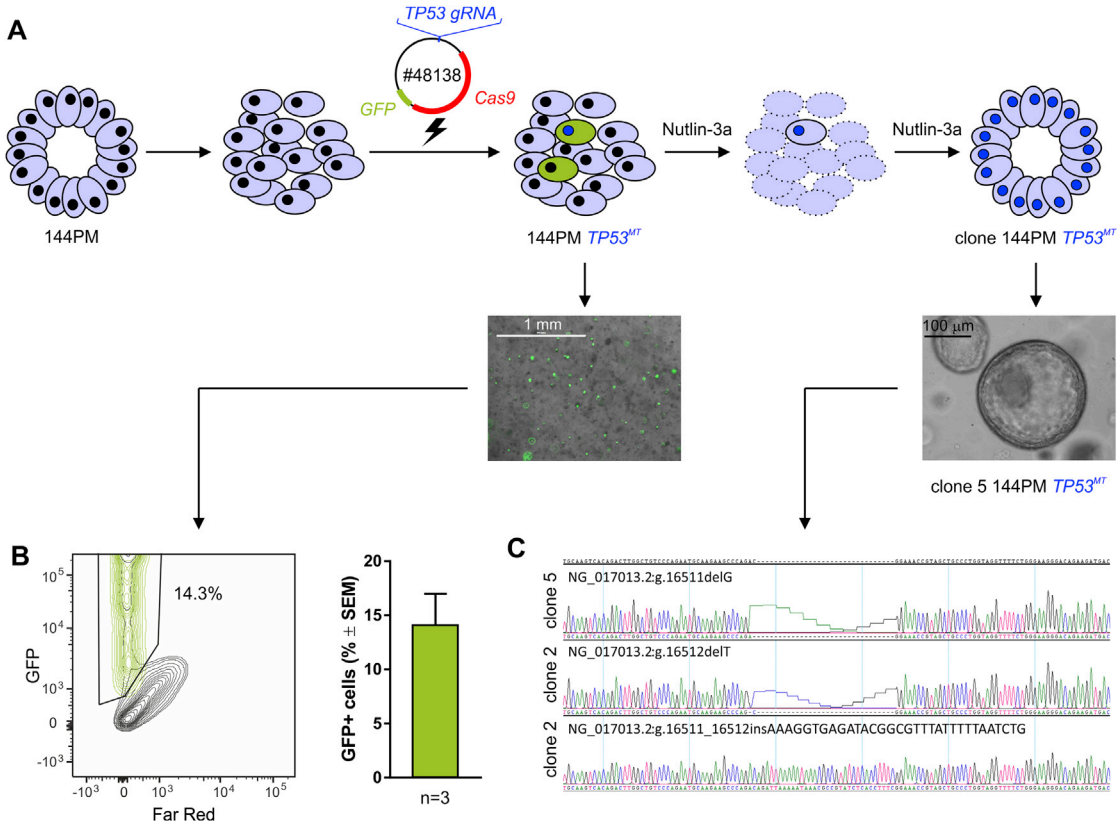


**Figure S4. Gene Editing of Mammary Gland Organoids, Related to STAR Methods**

(A) Scheme depicting the process of generating *TP53* mutant mammary gland organoids (dissociation, electroporation, selection, clonal outgrowth). Micrographs show representative examples of key points (electroporation, clonal outgrowth).

(B) Representative FACS plot and quantification of three electroporations showing efficient delivery of the Cas9 plasmid into mammary gland organoid cells.

(C) Sequence traces of the *TP53* region targeted by Cas9 in two Nutlin-3 resistant clones along with genotypes.